



Bard College

Bard Digital Commons

Senior Projects Spring 2025

Bard Undergraduate Senior Projects

Spring 2025

Modeling the Extra-Cellular Matrix in Cancer Angiogenesis

Nadia Mehjabin

Follow this and additional works at: https://digitalcommons.bard.edu/senproj_s2025



This work is licensed under a [Creative Commons Attribution-Noncommercial-No Derivative Works 4.0 License](#).

Bard

Modeling the Extra-Cellular Matrix in Cancer Angiogenesis

A Senior Project submitted to
The Division of Science, Mathematics, and Computing
of
Bard College

by
Nadia Mehjabin

Annandale-on-Hudson, New York
May, 2025

Abstract

Angiogenesis is a vital developmental process that supports tissue growth and repair; however, in cancer, it can accelerate tumor progression. The extracellular matrix (ECM) is a dynamic network of proteins and polysaccharides that provides structural and biochemical support to surrounding cells. The ECM regulates angiogenesis by influencing the direction of tip cell migration. This project builds on Dr. Norton's angiogenesis model by incorporating ECM interactions with endothelial cells through agent-based modeling. Computational analysis reveals significant differences in tip cell behavior across gradients, highlighting the role of the ECM in angiogenesis. These findings improve our understanding of the vascular dynamics driven by ECM in cancer progression.

Contents

Abstract	iii
Dedication	vii
Acknowledgments	ix
1 Introduction	1
1.1 Biology Background	2
1.1.1 Cancer	2
1.1.2 Angiogenesis	4
1.1.3 Extracellular Matrix Proteins	5
1.2 Modeling Background	6
1.2.1 Agent-Based Modeling and Simulation	7
1.2.2 Agent-Based Modeling on Cancer	8
1.2.3 Previous Work	11
2 Methods	13
2.1 Code Overview	13
2.2 VEGF-only Model Implementation	14
2.2.1 Initial Setup	14
2.2.2 VEGF Representation	14
2.2.3 Tip Cell Movement and Decision-Making	15
2.2.4 Anastomosis Implementation	16
2.2.5 Simulation Loop and Termination Conditions	16
2.3 ECM-only Gradient Model	17
2.3.1 Model Architecture	17

2.3.2	ECM Gradient Generation	18
2.3.3	Tip Cell Movement in ECM Environment	18
2.3.4	Path Tracking and History	19
2.3.5	Anastomosis in ECM-only Model	19
2.3.6	Simulation Control and Visualization	20
2.4	Merged (ECM and VEGF) Model	20
2.4.1	Model Overview	20
2.4.2	Simulation Environment	21
2.4.3	Tip Cell Movement Algorithm	21
2.4.4	Anastomosis Detection	22
2.4.5	Simulation Workflow	22
2.4.6	Current Implementation Status	22
3	Results	25
3.1	VEGF-only Model	25
3.2	ECM-only Model	35
3.2.1	Uniform Gradient	36
3.2.2	Radial Gradient	39
3.2.3	Linear Gradient	42
3.2.4	Mean Displacements	46
3.3	Merged (ECM and VEGF) Model	50
3.3.1	Uniform Gradient	50
3.3.2	Radial Gradient	51
3.3.3	Linear Gradient	52
3.3.4	Comparison between ECM-only Model and Merged Model	53
4	Discussions and Conclusions	57
4.1	Next steps	59
4.2	Personal Reflection	60

Dedication

Nadia, may you always remember the determination and passion that brought you here.
To Ammu, Abbu, my brother Anis and my uncle Jasim: Through every high and low, your
faith in me never wavered, and your presence was my anchor.

Ammu - Your sacrifices and endless care shaped who I am. I could not be here today without
you and all the hardships you endured for us, to ensure that we are successful in life.

Uncle Jasim, your kindness and quiet guidance have meant the world.

Anis - you have always set the bar high, pushed me to do better and challenged me in ways
that only a big brother can. You encouraged me, believed in me, and yes, annoyed me the
most - but you were always there, no matter what happened. I would not be here without that
constant presence.

I carry all your love with me in everything I do. From the depths of my heart, thank you.

Acknowledgments

I would like to thank my advisor, Dr. Kerri-Ann Norton, and Dr. Sven Anderson for their support throughout my senior year. In addition, I am grateful to all professors in the computer science department for equipping me with the tools and skills necessary to complete my senior project successfully. Finally, I want to acknowledge my research advisor, Matthew Greenberg, who created a supportive and collaborative space for me during the Bard Summer Research Institute 2023, when I discovered my deep interest and passion for computational modeling.

I am deeply grateful to my friends for their unwavering support, encouragement, and companionship throughout this journey. Their presence in both the brightest and most challenging moments has meant more than words can express.

1

Introduction

Cancer is characterized by uncontrolled proliferation of cells and several hallmark traits, such as unlimited replicative potential, the ability to invade and spread, and the evasion of growth suppressors [13]. Angiogenesis—the process of forming new blood vessels—supports tumor growth and metastasis. Angiogenesis is governed by the interactions between the extracellular matrix (ECM) and vascular cells. This includes complex molecular signaling, cellular migration, and structural remodeling that facilitate tumor expansion and progression. Previous work in Dr. Norton’s lab investigated the interaction between cancer and angiogenesis in triple-negative breast cancer, but did not include ECM interactions. In this project, we plan to develop an agent-based model (ABM) based on Dr. Norton’s angiogenesis model and then add the interaction of endothelial cells with the ECM. This project aims to add an extracellular matrix (ECM) module to an existing agent-based cancer model developed in Dr. Norton’s lab to understand the complex interactions between cancer, angiogenesis, and the extracellular environment.

The extracellular matrix (ECM) refers to a network of fibrous proteins and glycosaminoglycans (GAGs) [5]. As described by [5], ECM provides structural support for cells within a tumor, acting as a bridge between cells, and contributes to survival and differentiation signals. Women account for breast cancer (BC) for 25% of all cancer cases and 12% of all cancer cases worldwide [15]. ECM plays a crucial role in BC progression, invasion, and metastasis; therefore, elucidating the

role of ECM will help to design therapies targeting different components of ECM [15]. Therefore, having an accurate and realistic representation of the dynamics of the ECM in cancer cells is crucial for our model to yield realistic results.

This project aims to improve the model by adding an ECM module to better simulate tip cell migration under different ECM gradient structures: linear, uniform, and radial. First, a model with VEGF only was developed to study tip cell movement with vascular endothelial growth factor (VEGF) concentration included, allowing examination of VEGF-driven migration patterns. Secondly, a separate ECM-only model is created to analyze the movement of the tip cell in response to three different ECM density gradients, investigating how varying ECM distributions affect migration behavior. Finally, the VEGF-only model is integrated into the ECM model by including VEGF concentration with tip cell behavior and updating movement rules to incorporate ECM-guided migration.

1.1 Biology Background

1.1.1 *Cancer*

Cancer is one of the leading causes of death worldwide, responsible for nearly 10 million deaths in 2020, accounting for almost one in six deaths [45]. Cancer is the transformation of normal cells into tumor cells when they no longer follow the genetic/epigenetic rules that regulate growth and function. However, not all tumors are cancerous. Tumors can be benign, meaning that they do not spread to other parts of the body, or malignant, meaning that they are cancerous and capable of spreading to other tissues and organs.

Hanahan et al. identified six essential properties, or “hallmarks”, that cells must acquire to become cancerous [13]. These hallmarks include the sustained maintenance of proliferative signaling, the evasion of growth suppressors, the activation of invasion and metastasis, the enabling of replicative immortality, the resistance of cell death and the induction of angiogenesis [13]. The first hallmark, the sustained maintenance of proliferative signaling, is characterized by cancer cells generating their growth factors or becoming hypersensitive to external signals through three

main strategies: altering extracellular growth signals, modifying cell surface receptors, and disrupting intracellular circuits that process these signals, such as the Ras-MAPK pathway [13]. For example, cancer cells can produce growth factors such as PDGF or overexpress receptors like EGFR, allowing them to bypass standard regulatory mechanisms and continuously divide [13].

The second hallmark, evading growth suppressors, refers to tumor suppressor genes such as p53 and RB, which generally regulate cell proliferation and trigger apoptosis when cells are damaged, but cancer cells develop mutations that disable these genes, allowing unchecked growth and evasion of repair mechanisms or apoptosis [13, 19, 39, 42]. The third hallmark, activating invasion and metastasis, involves cancer cells invading surrounding tissues and metastasizing to distant sites by losing adhesion molecules such as E-cadherin and altering integrins, allowing local invasion through protease-like matrix metalloproteinases (MMPs) [13]. This process, known as the invasion-metastasis cascade, allows cancer cells to enter the bloodstream or lymphatic system, travel to new tissues, and form secondary tumors [10].

The fourth hallmark, enabling replicative immortality, allows cancer cells to divide indefinitely despite the telomere shortening that typically limits cell division. Cancer stem cells (CSCs) play a crucial role in the production of intact progenitor cells with intact telomeres, thus bypassing senescence and support continued growth [3, 13]. The fifth hallmark, resisting cell death, involves cancer cells evading programmed cell death (apoptosis) by disabling tumor suppressor genes such as p53, which generally trigger cell cycle arrest or apoptosis in response to damage [13]. This ability allows cancer cells to survive despite genetic abnormalities, contributing to uncontrolled proliferation and tumor growth. Finally, the last hallmark, the induction of angiogenesis, is crucial for tumors, which require an increased supply of nutrients and oxygen. Cancer cells achieve this by forming new blood vessels [13].

Among all the hallmarks of cancer, the most relevant to this project is the ability of tumors to induce angiogenesis. Since we aim to model angiogenesis, it is essential to understand how

cancer affects our blood vessels. In the next section, we discuss angiogenesis, the formation of new blood vessels in cancer, as well as its effects on tumor growth.

1.1.2 Angiogenesis

Like any other living cell, tumor cells require nutrients to survive and reproduce. The essential nutrients and oxygen necessary for tumor cells to live and proliferate come from blood vessels, also known as the vasculature [18]. As discussed above, one of the main hallmarks of cancer is the ability to recruit new blood vessels. In this way, if the tumor undergoes metastasis, it can maintain a supply of oxygen and nutrients as it migrates. The process of forming new blood vessels is known as angiogenesis. For a tumor to recruit new blood vessels, it needs to send a signal that triggers the formation of new blood vessels. This process is known as the “angiogenic switch”.

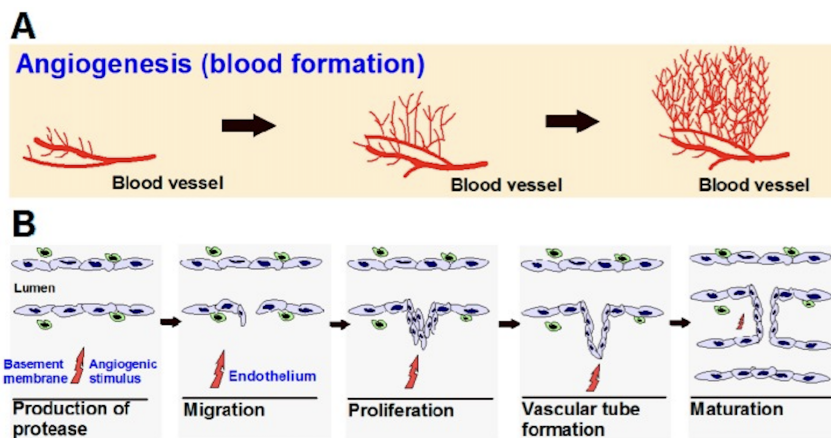


Figure 1.1.1: Steps in angiogenesis. This figure is taken from Rajabi et al. [35].

These new blood vessels are formed from preexisting blood cells via the “sprouting” of endothelial cells, thus expanding the vascular tree [35]. The sprouting angiogenesis mechanism (Figure 1.1.1) involves a series of events that are simulated and controlled by angiogenic growth factors, receptors, and inhibitors [35, 41]. As mentioned in [20], this process involves three different types of endothelial cells that contribute to the new vasculature: tip cells, stalk cells, and phalanx cells. A tip cell is a type of cell from the parent vessel that becomes the migratory leading cell. Tip cells migrate in response to vascular endothelial growth factor (VEGF), a key

protein secreted by tumor cells under hypoxic conditions. Stalk cells follow the tip cells and branch out from the parent vessel, establishing the vascular lumen and junctional connections to the forming sprout; phalanx cells support the sprout. The connection of the luminal space of the sprout with the parent vessel is known as lumen formation. The developing sprout then connects with other vessels through a process called anastomosis [20]. Once the new blood vessels undergo anastomosis, the tumor gains access to oxygen and nutrients, allowing it to survive and grow.

Angiogenesis occurs through two processes: sprouting angiogenesis and intussusceptive angiogenesis [41]. Our angiogenesis model only uses the idea of sprouting angiogenesis for simplicity of modeling. The long-term goal of this project is to incorporate different forms of angiogenesis and vessel stabilization. Unfortunately, it is not easy to observe vascular growth or its effect on a tumor in patients and in vivo models. It takes time for the capillaries to grow and the number of studies that observed this process from images is very low [37]. For these reasons, computational modeling is a commonly used tool to observe and predict the effects and patterns of angiogenesis. This allows us to make these predictions in a short amount of time.

1.1.3 *Extracellular Matrix Proteins*

The extracellular matrix (ECM) is a three-dimensional noncellular network of collagens, laminins, elastins, elastic fibers, glycoproteins, and proteoglycans [13]. It provides structural support to cells and regulates various cellular processes, such as growth, migration, differentiation, survival, homeostasis, and morphogenesis [19]. Each type of tissue, connective tissue, cartilage, or bone, has a different composition of the ECM, its components being produced and organized by resident cells to meet the specific requirements of that tissue (as reviewed in [19]). ECM is a dynamic structure that undergoes continuous remodeling that consists of the deposition, degradation, and modification of its components. Therefore, abnormal behavior of the ECM leads to pathological changes, including tissue fibrosis and cancer [24, 26].

In cancer, the properties of the extracellular matrix (ECM) change significantly compared to normal tissues. Cancer cells contribute to the remodeling of the ECM, creating a microenvironment that allows the tumor to expand. As tumor cells proliferate, the surrounding ECM undergoes architectural changes, including increased secretion of fibronectin and collagens I, II, III, and IV [43]. Because of that, tumor progression requires continuous interaction between the ECM and tumor cells, resulting in enhanced growth factor signaling [43]. Enzymes such as matrix metalloproteinases (MMPs), cathepsins, and elastases break down ECM proteins [42]. This degradation not only alters the structural integrity of the ECM, but also releases growth factors. By improving vascular endothelial growth factor signaling in endothelial cells (EC), the stiffness of the ECM increases angiogenesis, resulting in cancer progression [25]. Therefore, remodeling of the ECM is an integral part of the angiogenic process [5].

The intricate interactions between ECM proteins, cellular processes, and tumor progression underscore the critical role of the extracellular matrix in cancer biology. The dynamic nature of ECM, characterized by continuous remodeling and protein interactions, elicits biochemical and biophysical signals to influence cell adhesion and migration [43]. In the context of cancer and angiogenesis, the ECM becomes more than a passive structural network: it becomes an active participant in tumor progression. The complex interplay between ECM proteins, growth factors, and cellular signaling pathways creates a fertile ground for tumor expansion, metastasis, and vascular development [7, 17, 38]. Understanding these nuanced interactions is crucial to developing targeted therapeutic strategies that can potentially disrupt the supportive microenvironment of cancer cells.

1.2 Modeling Background

In this section, we explain different types of computational model, go over angiogenesis models and ECM models, and discuss the previous work of Dr. Norton’s computational biology lab at Bard College.

1.2.1 Agent-Based Modeling and Simulation

Agent-based modeling and simulation is a computational model implemented as a computer simulation in which there are individual entities and their behaviors and interactions. In ABMS, systems are characterized by autonomous and independent entities known as agents performing actions and interactions in the simulation environment, the virtual world, to create an experimental model *in silico* [1]. An agent must be identifiable, which means that it has to be distinguishable from its environment by some kind of spatial, temporal, or functional attribute [32]. The behavior of each agent is described through sets of rules, which can be either probabilistic or deterministic and may depend on internal and external variables: the first account for the intrinsic dynamics of the agent and the latter for the effects of the surrounding environment and neighboring agents [1, 4, 9]. Importantly, system behavior is not reduced to the mere superposition of its elementary components but emerges from concurrent agent actions, interactions, mutual influence with the environment, and feedback loops that dynamically evolve throughout the simulation [6].

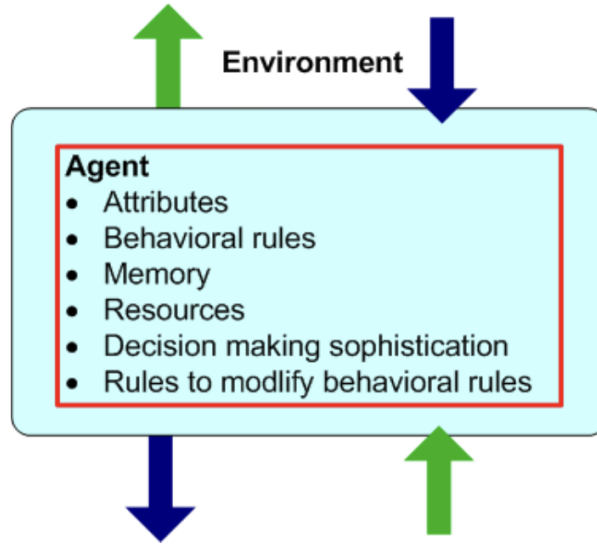


Figure 1.2.1: A typical agent: This figure is taken from Macal et al.[21].

For practical modeling purposes, agents need to have certain properties and attributes. An agent is autonomous and self-directed, modular or self-contained, social, interacting with other

agents, may live in an environment, has explicit goals that drive its behavior, can learn and adapt its behavior based on its experiences, and, lastly, has resource attributes (Figure 1.2.1) [21]. Computational modeling is a method of recreating real-world scenarios and interactions. There are different types of model available in the computational biology field, such as continuous modeling, game theory-based modeling, hybrid modeling frameworks, and agent-based modeling. The benefit of computational models is that they can simulate and predict the development of biological phenomena across multiple spatial and temporal scales, but also integrate information from well-established *in vitro* and *in vivo* models, and test new hypotheses in cancer biomedicine [8].

ABM stands out among computational modeling approaches because it allows for a detailed representation of cellular-level interactions, which are essential for this project. Agents in ABM can represent biological entities, such as cells or vessels, with their behaviors governed by mathematical rules. For example, cells (agents) interact with other cells and their environment, modeled as Markov processes, where transitions to new states depend only on their current state [8]. In this project, ABM will be used to simulate vessel interactions at the cellular level and to incorporate environmental behaviors, which are critical to understanding how the density of ECM influences the development of tumor vasculature. The flexibility of ABM makes it an ideal framework for investigating these processes dynamically and mechanistically.

1.2.2 Agent-Based Modeling on Cancer

Agent-Based Models are used to simulate cancer. Each cancer cell is programmed to be an independent agent with proliferation, migration, and death rates. This allows the researcher to track the development, growth, branching, and morphology of tumors on a cellular level.

Each cell makes decisions based on some sort of decision tree, where each decision depends on information collected from the cell's parameters or the environment. For example, Figure 1.2.2 from another cancer ABM shows how each cancer cell agent makes decisions [27]. At first, each cell checks if there is free space; if so, it can migrate; otherwise, it becomes quiescent. Migration

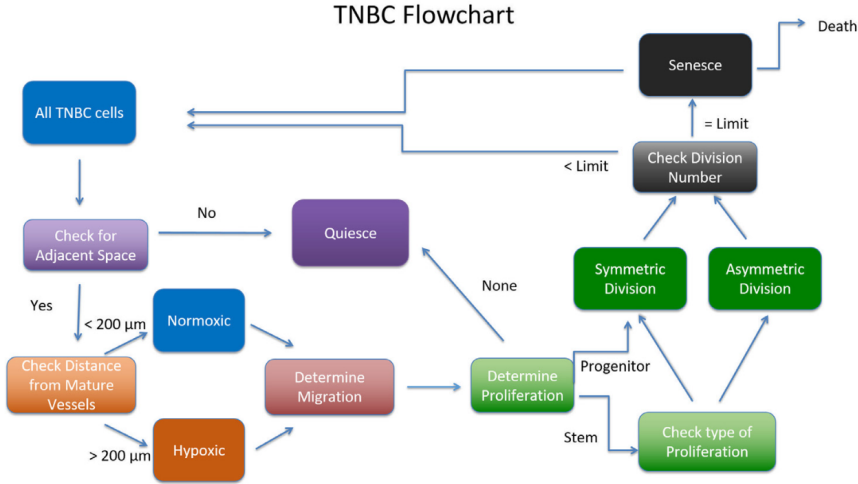


Figure 1.2.2: Sample AMB Flowchart. This figure is adapted from Norton et al.[27].

decisions are influenced by three key factors: CCR5 expression levels, hypoxic conditions, and proximity to stromal cells. Similarly, the proliferation potential is determined by evaluating the characteristics of stem cells, oxygen availability, and proximity to stromal cells. When proliferation occurs, stem cells can divide symmetrically or asymmetrically, while progenitor cells are restricted to symmetric division only. Following these processes, each cell evaluates and updates its oxygen status, categorizing itself as hypoxic or normoxic. Finally, cells in senescent states face a probability-based mortality check, with some dying during each simulation cycle.

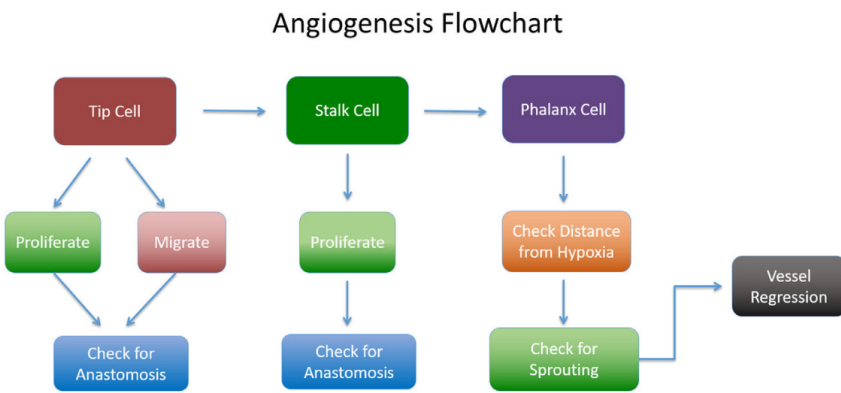


Figure 1.2.3: Sample AMB Flowchart. This figure is adapted from Norton et al. [27].

In the angiogenesis process of Figure 1.2.3, each tip cell checks if it has neighboring stalk cells; if not, it proliferates to produce a stalk cell [27]. Otherwise, it migrates on the basis of the local

VEGF concentrations. Stalk cells can proliferate if they have reached their cell cycle. If there are hypoxic tumor cells in proximity to the vessel, then branching will occur.

Agent-based cancer models have led to interesting results and breakthroughs. For example, [30] used a multiscale 3D agent-based modeling approach to examine tumor growth and angiogenesis in breast cancer, with a unique inclusion of tumor and normal tissue cells. The results showed that their computationally efficient discretized approach to nutrient flow produced similar outcomes to more complex models, with tumors growing in expected spheroid patterns and demonstrating significantly enhanced growth when angiogenesis was enabled. Another model identified that high VEGF-A disrupts vascular patterning, VEGF gradients enhance tip cell selection, and Dll4/VEGFR-2 proteins oscillate in environments with high VEGF [2]. This study uses a hierarchical agent-based model to simulate a feedback loop between VEGF-A tip cell induction and Dll4/Notch-mediated lateral inhibition. Another study shows modeling angiogenesis by examining the balance between stochastic (random) and deterministic (rule-based) influences [44]. It develops an agent-based model (ABM) to simulate the initiation and location of endothelial cell sprouts, comparing its accuracy to a purely stochastic Monte Carlo model. The findings suggest that rule-based approaches better capture the complex mechanisms underlying angiogenesis than purely random simulations.

Various levels of mathematical modeling exist to include how capillaries are formed, blood flow, vessel adaptation, and the extent to which chemical diffusion reaches the tissue. This study analyzes how drugs can be sent to the tumor through the formed vessel network, based on the quality of the created vessels [22]. They found that the simulation was sensitive to changes in parameters for the haptotactic response of blood vessel cells, blood viscosity, and blood pressure, and that the tracer drug sent through the system was able to travel more easily through well-formed vessels [22]. Another study uses a two-dimensional multiscale model of angiogenesis in which endothelial cell sprouting occurs due to VEGF diffused by healthy cells [31]. Sprouts grow based on a VEGF gradient that occurs when cells do not have enough oxygen. Sprouts die if they do not create a loop within a given period and are only active once it is a viable

segment. They find that a larger number of tumor cells causes a higher vascular density and that network remodeling requires a balance between angiogenesis and vessel pruning. A two-dimensional PDE model of tumor growth with angiogenesis has also been developed [36]. They find that asymmetrical tumor growth leads to a greater degree of branching at the surface of the tumor compared to symmetrical tumor growth.

1.2.3 Previous Work

In this section, we discuss previous work done in Dr. Norton’s lab that led to the development of this project. This section will not focus on angiogenesis modeling. Instead, we will review some of the previous related studies that used agent-based models to study triple negative breast cancer (TNBC).

A previous paper by Norton et al. 2017 used a computational model, which is an agent-based in silico simulation that starts with 100 triple negative breast cancer cells, specifically MDA-MB-231, placed on a cubic grid [29]. This model incorporates parameters such as CCR5 expression levels and stem cell fractions to simulate tumor growth, migration, and interactions within the microenvironment. The model evaluates different conditions, including drug treatments and hypoxia, to understand their effects on tumor morphology and growth dynamics. The purpose of the model was to examine the effects of CCR5+ cancer cell migration, stem cell proliferation, and hypoxia on the growth and progression of triple negative breast tumors. The results indicated that the percentages and proliferation rates of stem cells significantly impact tumor growth and treatments that do not eliminate all stem cells lead to tumor relapse, while hypoxia accelerates tumor growth. Furthermore, maraviroc treatment slightly reduced tumor size but was less effective than antistem cell treatments or in addressing hypoxia.

Another paper by Norton et al. developed an agent-based model that integrates a triple negative breast cancer model with an angiogenesis model, focusing on interactions between cancer-associated stromal cells, including macrophages and fibroblasts [27]. Simulate tumor growth, vasculature response to hypoxia, and differentiate monocyte recruitment to macrophages, allow-

ing analysis of tumor progression and the role of the tumor microenvironment. The model also examines the effects of macrophage infiltration and angiogenesis on cancer cell behavior and tumor heterogeneity. The agent-based model consists of a cellular grid ($100 \times 100 \times 100 \mu\text{m}$) for tumor cells and a vascular grid ($2000 \times 2000 \times 2000 \mu\text{m}$) for blood vessels, with specific voxel sizes to accurately represent cellular structures. It tracks various cell types, including 100 tumor cells (20 cancer stem cells and 80 progenitor cells), macrophages, fibroblasts, and capillaries, with each simulation iteration representing approximately 6 hours of real time. The model incorporates mechanisms for the assessment of hypoxia based on the distance to the vasculature, angiogenesis processes such as tip cell migration and stalk cell proliferation, and dynamic interactions between tumor cells and the stroma, allowing for a comprehensive analysis of tumor growth and microenvironment interactions.

From the study by Campbell et al. [5], we know that ECM proteins directly and indirectly regulate angiogenesis. These proteins impact tumor progression by modulating proangiogenic factors such as vascular endothelial growth factor (VEGF) and basic fibroblast growth factor (bFGF). The influence of ECM on angiogenesis emphasizes the importance of understanding the tumor microenvironment in cancer progression. This led to the development of my senior project, where we developed an ECM model to find the influence of tip cell movement by VEGF concentration and ECM density.

2

Methods

The computational lab of Dr. Norton has developed previous agent-based models of triple negative breast cancer [28, 29]. Those previous simulations include tumor cells, the vasculature (blood vessels), immune cells, and other cells in tumor microenvironments. The simulations of the blood vessels did not account for the factor of the extracellular matrix (ECM). The goal of this project is to incorporate ECM gradients in angiogenesis to observe tip cell migration. We have designed three separate ABM models: VEGF-only, ECM-only, and Merged (ECM and VEGF) models.

2.1 Code Overview

The computational model implemented in this study simulates angiogenesis, focusing on the formation of vascular networks in response to growth factors (VEGF) and extracellular matrix (ECM) interactions. We developed a VEGF-only, ECM-only model and a Merged (ECM and VEGF) model. These models employ a grid-based approach where cells navigate through a two-dimensional environment guided by various biochemical and biophysical cues. The VEGF-only model is a preliminary model designed to understand the implementation of the angiogenesis process. In the ECM-only model, the ECM environment is designed in three different gradients: linear, radial, and uniform. These gradients represent how the ECM density is distributed in the model. In this study, we examine how the distribution of ECM contributes to differences in tip

cell migration. The Merged model is also a preliminary model for exploring tip cell migration, where ECM and VEGF concentration play an important role in migration.

The simulation framework of the models consists of a main execution script that handles the simulation parameters, initialization, execution, and visualization. The behavior of the tip cells was defined in classes that encapsulated the biological behavior of the endothelial tip cells in cancer scenarios. After each simulation, the results were saved as data files. The simulation operates step by step, alternating between growth phases and anastomosis check phases, with the state of the system visualized at the end of the simulation. Our resulting model implementation allows for the analysis of how different factors influence the formation patterns of the vascular network.

2.2 VEGF-only Model Implementation

2.2.1 Initial Setup

The angiogenesis model utilizes a 50×50 dual-grid system to track both vessel types and unique vessel identities simultaneously. In the initialization of the Vasculature class (there is only one class), two primary grids are established: the main grid tracks cell types (empty = 0, mature vessel = 1, tip = 2), while the gridID array assigns unique numerical identifiers to each growing vessel. The model begins with predefined initial cell positions at the tip, which are stored along with individual growth trajectories in the `cell_paths` dictionary. Each tip cell is given a unique identifier starting from 1, and its state is tracked through the `active_tips` list, which indicates whether each tip is still capable of growth. This structured approach enables precise tracking of vessel growth and supports complex interactions such as anastomosis events between separate vessels.

2.2.2 VEGF Representation

The model incorporates a concentration field of Vascular Endothelial Growth Factor (VEGF) as a key driver of angiogenic sprouting. This field is represented as a two-dimensional array that

matches the dimensions of the grid, with initial values randomly distributed between 0 and 1 throughout the simulation space. As vessels grow, they interact with and modify this VEGF field: tip cells consume VEGF at their current positions (reducing the concentration by 50%), and the entire field undergoes a global decay of 5% during each growth step, simulating the natural degradation of growth factors. This implementation creates a dynamic environment in which vessel growth follows chemical gradients, with tips preferentially moving toward locations with a higher VEGF concentration. The model selects growth directions by identifying neighboring positions with maximum VEGF values from among the valid movement options.

2.2.3 Tip Cell Movement and Decision-Making

The movement of the tip cell follows a directionally biased and context-dependent decision-making process. The `get_valid_neighbors` function implements directional persistence for tip cell migration in an angiogenesis simulation. This function identifies which grid positions a tip cell can potentially move to next based on its current position and movement history. For the first move of a cell, it considers all 8 surrounding positions (four cardinal directions plus diagonals). For subsequent moves, it uses the previous position of the cell to determine its movement direction (dx , dy) and then selects a specific set of neighboring forward bias positions based on that direction, which favors continued movement in similar directions. This approach mimics the biological tendency of endothelial tip cells to maintain directional persistence during blood vessel formation. The function then filters these potential positions to remove any that would be outside of the grid boundaries or that already contain vessel cells. The resulting list of valid neighbors is used by the growth algorithm to determine where the tip cell can move next, creating a biologically realistic pattern of blood vessel formation.

Then, in the `grow` function, for each active tip cell, the valid neighbors consume Vascular Endothelial Growth Factor (VEGF) at that location, and then identify valid neighboring positions for potential growth. The direction of growth is determined by the highest concentration of VEGF among available neighbors, with random selection if multiple positions have the same

maximum value. Once a new position is selected, it is marked as a tip cell in the grid, assigned the same ID as its parent, and added to the appropriate data structures, including path trajectories. If no valid neighbors exist or the tip reaches a boundary, the tip becomes inactive. This process effectively models how endothelial tip cells follow chemical gradients to form new blood vessels during angiogenesis.

2.2.4 Anastomosis Implementation

Anastomosis, the vessel fusion process, is implemented through the `check_anastomosis` function that operates in alternating steps of the simulation. This function examines two critical conditions for vessel fusion: tip-to-tip encounters (when tips from different vessels are within Manhattan distance 2 of each other) and tip-to-existing-vasculature encounters (when a tip comes adjacent to a mature vessel segment of a different ID). The function `is_near` serves as a helper method to calculate the Manhattan distance, which measures the total distance traveled along a grid by calculating the combined horizontal and vertical distance covered between the tips. Manhattan distance is the sum of the absolute differences of the coordinates:

$$\text{Distance}_{\text{Manhattan}} = |x_1 - x_2| + |y_1 - y_2|$$

When anastomosis is detected, the involved tip cells are converted to mature vessels, deactivated from further growth, and the event is recorded with detailed information, including the positions and vessel IDs of the connecting elements. The `anastomosis_events` list maintains a history of all connections, which is later visualized in the simulation output. This implementation allows the formation of complex vascular networks with realistic connectivity patterns that emerge naturally from the growth and interaction rules.

2.2.5 Simulation Loop and Termination Conditions

The simulation progresses through a defined number of steps (default 200), alternating between growth and anastomosis-checking phases. During even-numbered steps, the `grow()` method

advances active tip cells, while odd-numbered steps invoke `check_anastomosis` to detect potential vessel connections. Throughout the simulation, comprehensive data are collected on vessel positions, VEGF values, displacement from initial positions, and anastomosis events. The system creates visualizations at regular intervals, showing vessel development, ID distribution, and VEGF concentration patterns. The simulation ends after completing all steps and the final analysis calculates metrics that include vessel displacement and status (active, anastomosed, or inactive). The results are systematically saved in files, including step-by-step images, a summary file with key statistics, and a TSV data file containing detailed vessel parameters. This structured output facilitates a quantitative analysis of the properties of the emerging vascular network.

2.3 ECM-only Gradient Model

2.3.1 Model Architecture

The computational model implements a grid-based approach to simulate endothelial tip cell migration through extracellular matrix (ECM) environments. The model architecture employs a modular design that separates gradient generation, cell movement mechanics, path tracking, and anastomosis detection into distinct components.

Three gradient types were implemented to represent different ECM environments: linear, radial, and uniform. Each gradient type is parameterized to allow customization of physical properties such as slope and intercept for linear gradients, center value and decay rate for radial gradients, and consistent density for uniform gradients. This flexible parameterization facilitates systematic exploration of how ECM heterogeneity affects tip cell migration patterns.

The initialization process establishes a 2D grid of specified dimensions, generates the appropriate density gradient of the ECM, and places the initial tip cells at designated positions. Each tip cell is assigned tracking metadata to record its movement history and activity status.

2.3.2 ECM Gradient Generation

In the angiogenesis simulation, three distinct gradient configurations of the extracellular matrix (ECM) were implemented to evaluate their influence on the migration of tip cells and the formation of vascular patterns. The first is the uniform ECM gradient, where the ECM density remains constant throughout the simulation space, providing a baseline to understand cell behavior in the ECM. In this gradient, by default `uniform_value = 0.5`. The second setup is the linear gradient, in which the ECM density changes gradually along a defined axis, typically decreasing along the x-direction. This mimics a directional ECM remodeling scenario and allows assessment of guided migration due to substrate stiffness.

$$\text{linear_gradient} = \text{slope} \times \text{x_coordinates} + \text{intercept} \quad (2.3.1)$$

$$\text{radial_gradient} = \text{center_value} \times \exp(-\text{decay_rate} \times \text{distances}) \quad (2.3.2)$$

The third setup, the radial gradient, features an ECM density that is higher in the center, and as the distance increases, the density decreases, where the `decay_rate` is a constant parameter. This setup is intended to reflect biological conditions, such as peritumoral degradation of ECM, guiding tip cells toward or away from tumor-like sources.

2.3.3 Tip Cell Movement in ECM Environment

The tip cell movement algorithm implements a biologically inspired directional persistence model. Movement decisions are based on three key factors:

1. ECM Density Sensing: Tip cells preferentially move toward regions of lower ECM density, simulating the proteolytic activity of real endothelial tip cells that cleave dense ECM to facilitate migration.
2. Directional Persistence: Rather than random exploration, cells exhibit directional memory from previous movements. This persistence is implemented through a neighbor selection

system that prioritizes forward bias positions based on the previous movement vector of the cell.

3. Decision-Making Process: For each movement step, the algorithm identifies valid neighboring positions based on directional constraints, evaluates the ECM values at these positions, selects the position with the lowest ECM density, with built-in randomization to resolve ties, and updates the cell's position and status.

A special case exists for the first movement, where directional constraints are relaxed, allowing cells to sample all eight neighboring positions (cardinal and diagonal positions). This captures the initial exploratory behavior before direction persistence is established.

2.3.4 Path Tracking and History

The model maintains comprehensive tracking of the cell movement history using a dictionary-based data structure. Each tip cell is associated with a path, an ordered list of coordinates that represents its trajectory from initialization to its current position. This path tracking serves multiple purposes, such as completing historical records of cell trajectories, which enable post-simulation analysis of migration patterns; previous positions inform future movement decisions, creating biologically realistic path continuity; paths represent the vasculature network forming behind the advancing tip cells; and path data enable detection of potential anastomosis events between different vessel branches. The tracking system also maintains the state of each tip cell, including the active/inactive status and whether it has completed its first movement step.

2.3.5 Anastomosis in ECM-only Model

Anastomosis detection implements a two-phase approach to identify and process vessel fusion events. The algorithm can detect two types of anastomosis, such as tip-to-tip anastomosis, when two actively migrating tip cells come within a defined proximity (distance ≤ 2), and tip-to-vessel anastomosis, when a tip cell approaches an existing vessel segment formed by another tip cell (distance ≤ 1). As active tip cells migrate, they are evaluated for potential collisions with

other vessels or tips. Upon detection of anastomosis, tip cells are deactivated and the event is recorded. The anastomosis detection algorithm runs alternately with the movement steps in the simulation, mimicking the biological process where vessels grow, then connect, and then continue to grow from other active tips.

2.3.6 *Simulation Control and Visualization*

The simulation framework implements a systematic approach to experiment control and data collection. The system accepts parameters for the type of gradient, the size of the grid, the initial positions of the tip, and the number of simulation steps. The simulation records the positions of the tip cells at each time step, the ECM values encountered by each cell, anastomosis events, and cell displacement metrics. The results are systematically saved as TSV files containing position, ECM values, displacement, and anastomosis counts. For visualization plots, Matplotlib is used; plots show the ECM gradient, cell paths, and anastomosis events. This comprehensive data collection approach facilitates quantitative analysis of how different gradient patterns in ECM influence vessel network formation, tip cell migration efficiency, and anastomosis frequency.

2.4 Merged (ECM and VEGF) Model

2.4.1 *Model Overview*

The Merged model is designed to simulate the movement of endothelial tip cells during angiogenesis, taking into account both extracellular matrix (ECM) density gradients and vascular endothelial growth factor (VEGF) concentration. The model implements a computational framework in which tip cells navigate through a two-dimensional environment, making movement decisions based on the density of the ECM and the concentration values of VEGF in neighboring positions. It also incorporates anastomosis detection, allowing the identification of connections between growing vessel sprouts.

2.4.2 *Simulation Environment*

The simulation environment consists of a two-dimensional grid that represents the space in which angiogenesis occurs. The environment incorporates two key components: the ECM density grid and the VEGF concentration grid. The ECM grid is generated similar to the ECM-only gradient model architecture. Linear gradients, which vary linearly across the x-direction with configurable slope and intercept. Radial gradients, which vary based on the distance from the center, with a configurable center value and decay rate. Uniform gradients that maintain a constant value across the entire grid. VEGF concentration is implemented as a randomly distributed grid of values between 0 and 1, representing varying concentrations of growth factor throughout the environment. This implementation mimics the heterogeneous distribution of growth factors that is often observed in biological tissues.

2.4.3 *Tip Cell Movement Algorithm*

The tip cell movement algorithm is based on the principle that endothelial cells preferentially migrate to regions with lower extracellular matrix (ECM) density, which may be easier to navigate, and higher VEGF concentration, which serves as a chemoattractant. The algorithm begins by identifying valid neighboring positions based on the current location of the cell and the previous direction of movement. For each valid neighbor, it assesses the ECM density and VEGF concentration levels.

The algorithm then determines which positions have the lowest ECM values and which have the highest VEGF concentrations. If a single position satisfies both conditions -having both the lowest ECM and the highest VEGF - it is selected as the next position. If no such position exists, the algorithm randomly selects from among the positions with the lowest ECM and the highest VEGF, and calculates the average of their coordinates to determine the next location. The tip cell then moves to this new position and updates its movement path accordingly.

To ensure biologically realistic vessel growth, the model imposes directional constraints that prevent sharp turns and backtracking. During the initial movement, all eight neighboring po-

sitions (including the cardinal and diagonal directions) are considered valid. However, for subsequent movements, the set of valid neighbors is restricted according to the previous direction, creating a forward-biased migration pattern that reflects the observed behaviors in angiogenic sprouting.

2.4.4 Anastomosis Detection

Anastomosis, the formation of connections between vessel segments, is an important aspect of angiogenesis that contributes to the development of functional vascular networks. The model implements anastomosis detection, similar to the VEGF-only and ECM-only models, through two primary mechanisms. Tip-to-tip anastomosis: Detection of cells of the active tip that come within a specified distance of each other (distance ≤ 2). Tip-to-vessel anastomosis: Detection of cells of the active tip that come within a specified distance of existing vessel segments (distance ≤ 1). When anastomosis is detected, the involved tip cells are deactivated, preventing further migration, and the anastomosis event is recorded. This mechanism allows for the formation of closed loops in the vascular network, which enhances its connectivity and potential for flow.

2.4.5 Simulation Workflow

The simulation proceeds in alternating phases of movement and anastomosis detection: In even numbered steps, the tip cells move according to the movement algorithm. In odd-numbered steps, the model checks for anastomosis events. The simulation continues until either a specified number of steps is reached or all the tip cells become inactive. This alternating approach allows for both the growth and connection of the vascular network, mimicking the biological processes of vessel sprouting and anastomosis.

2.4.6 Current Implementation Status

It should be noted that the current implementation represents a preliminary stage of the model. Although the core logic for tip cell movement and anastomosis detection has been successfully

implemented, there are some issues with the visualization plots that need to be addressed in future iterations. However, the underlying data generation and cell behavior algorithms work correctly, producing valid simulation results that can be analyzed to understand angiogenic processes.

The model has been designed with flexibility in mind, allowing for adjustment of various parameters such as gradient types, movement constraints, and initial cell positions of the tip. This flexibility facilitates the exploration of different angiogenic scenarios and the investigation of how various factors affect vessel formation and network development.

3

Results

This project aims to create an extracellular matrix model (ECM) to see how the density of the ECM affects the migration of tip cells. In the process of building this model, we programmed three different models to lead to the main goal, which is to evaluate how VEGF and ECM density concentration affect tip cell migration. We started with a simple VEGF-only model in 2D and then an ECM-only model of three different gradients in 2D, and lastly, the merged model (ECM and VEGF). In this section, we discuss the visualizations and findings of each model mentioned above.

3.1 VEGF-only Model

The VEGF-only model is simulated in progressive iterations to better understand the interaction of tip cell migration with the level of VEGF concentration.

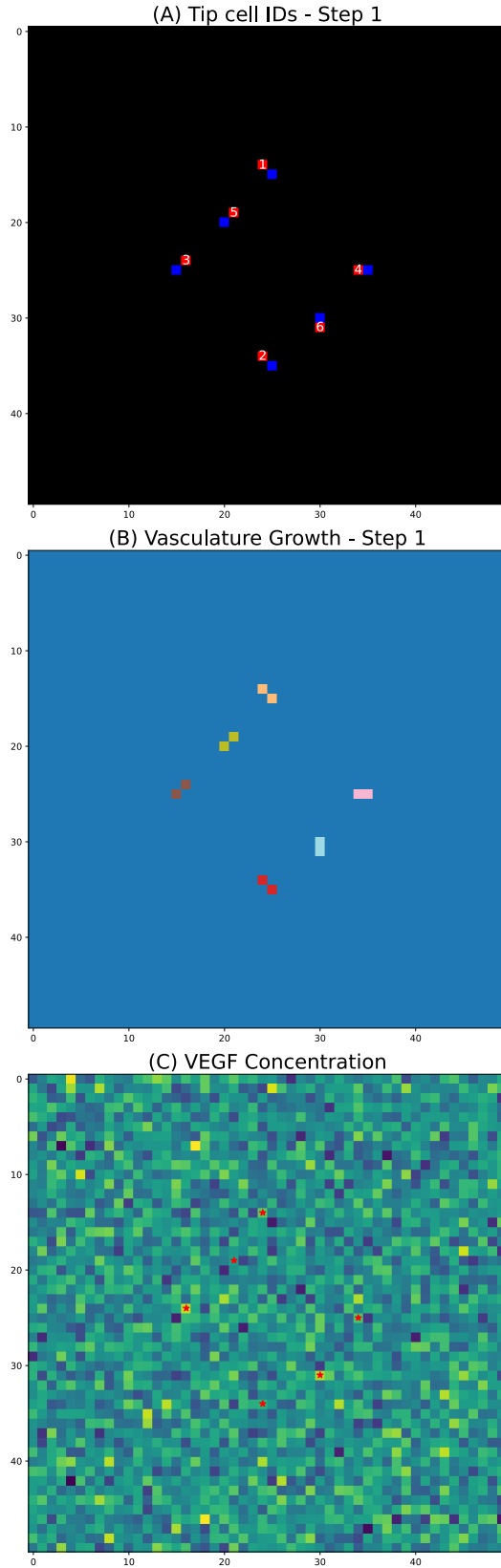


Figure 3.1.1: Step 1. (A) shows tip cell positions and identities (numbered in red), (B) displays vasculature growth patterns with different branch colors representing distinct cell lineages, and (C) shows the underlying VEGF concentration gradient as a heatmap.

Figure 3.1.1 shows that the angiogenesis simulation employed a 50×50 grid representing a standardized tissue domain in which vessel growth could occur. Each cell in the grid corresponds to a discrete spatial unit in which vessels could navigate and the VEGF concentration could vary. The simulation progressed through 200 discrete time steps, each step representing an iterative cycle of assessment of the tip of the vessel, directional decision making, and growth execution. As Figure 3.1.1 shows, the model was initialized with six strategically positioned vessel tips on the grid, each assigned a unique identifier (ID 1-6) for tracking purposes.

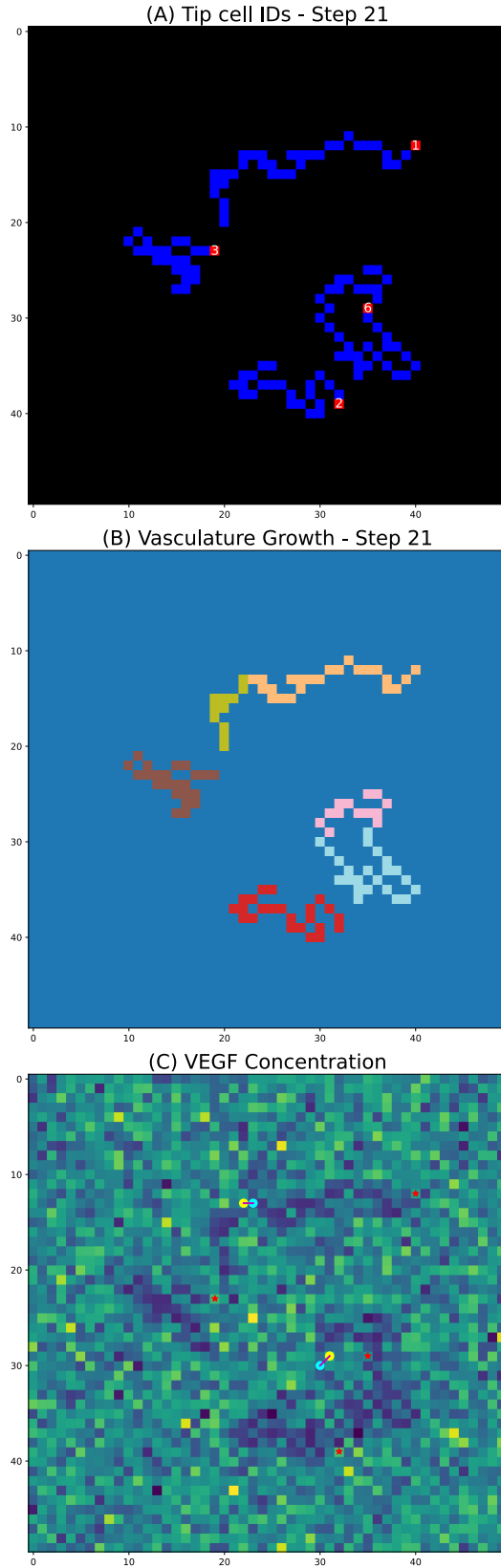


Figure 3.1.2: Step 21. The comparison between Step 1 and Step 21 demonstrates the temporal evolution of the vascular network, with initial tip cells extending into branching structures that follow local VEGF cues.

In step 21 of the 200-step angiogenesis simulation, four blood vessel tips (IDs 1, 2, 3, and 6) grow through the tissue following the VEGF concentration gradients (Figure 3.1.2). Each tip analyzed its surrounding grid positions based on its previous movement direction, creating a set of forward-biased neighboring positions that are checked for validity against grid boundaries. The algorithm then calculates the VEGF value at each valid neighboring position and identifies which position has the maximum concentration. In Figure 3.1.2, the tip of vessel 1 moves from position (14, 38) to (13, 39) and then to (12, 40), following the highest VEGF concentration path. Similarly, the other three tips select their next positions based on the same principle, with vessel 2 moving to (39, 32), vessel 3 to (23, 19) and vessel 6 to (29, 35). This process simulates how real blood vessels grow preferentially toward areas with higher concentrations of growth factors, demonstrating the fundamental mechanism of angiogenesis in which vessels extend toward tissues requiring an increased blood supply.

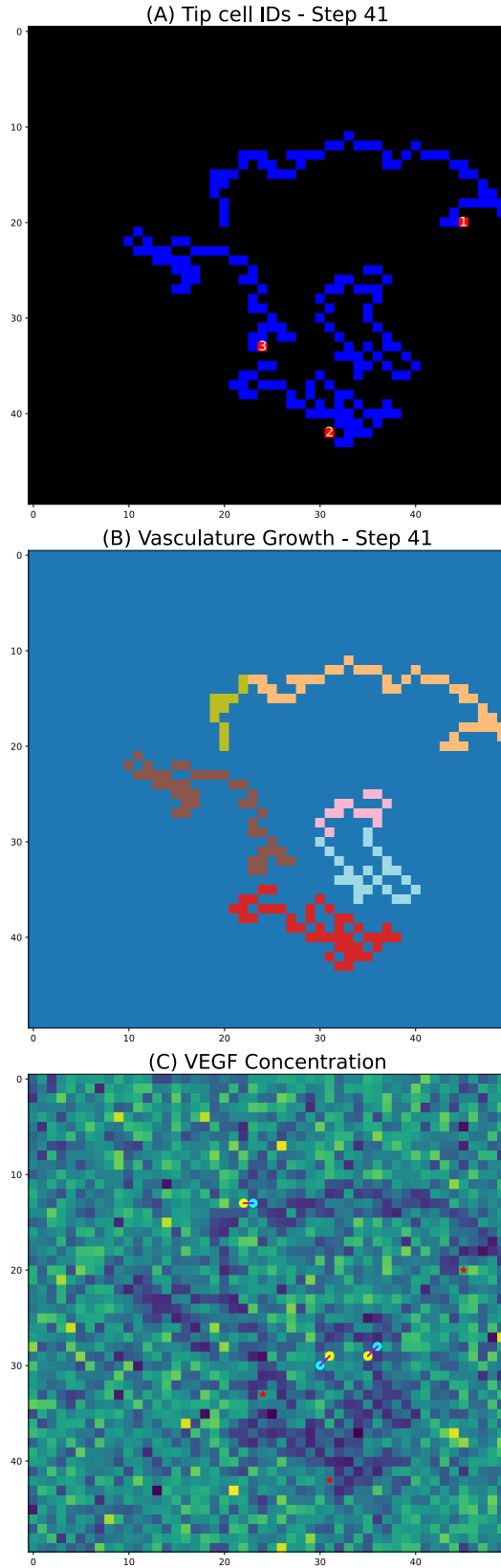


Figure 3.1.3: Step 41. The comparison between Step 21 and Step 41 demonstrates the temporal evolution of the vascular network, with initial tip cells extending into branching structures that follow local VEGF cues and forming new blood vessels.

From Figure 3.1.3, at step 41, we observe the growth behavior of the three tips of the vessel that navigate the distribution of vascular endothelial growth factor (VEGF). Each tip of the vessel follows a sophisticated decision-making process to determine its next position based on the previous direction of movement and the local concentrations of VEGF. Vessel 1, initially at position (20, 43), first evaluates five potential neighboring positions, calculating the VEGF values at each location. It selects position (20, 44) with the highest VEGF value of 0.215763, then proceeds to grow further to position (20, 45) with a VEGF value of 0.222. Similarly, vessel 2 at position (43, 33) analyzes its surroundings, identifies position (43, 32) as having the maximum VEGF concentration of 0.182127, and eventually extends to position (42, 31) with a VEGF value of 0.160. Vessel 3, starting at (32, 23), follows the same pattern by evaluating five neighbor positions, selecting (33, 23) with the highest VEGF value of 0.203893, and finally growing to position (33, 24) with a VEGF value of 0.189. The simulation demonstrates how vessel growth is directed by both previous movement vectors and local growth factor gradients, prioritizing areas with higher VEGF concentrations to simulate realistic angiogenesis behavior.

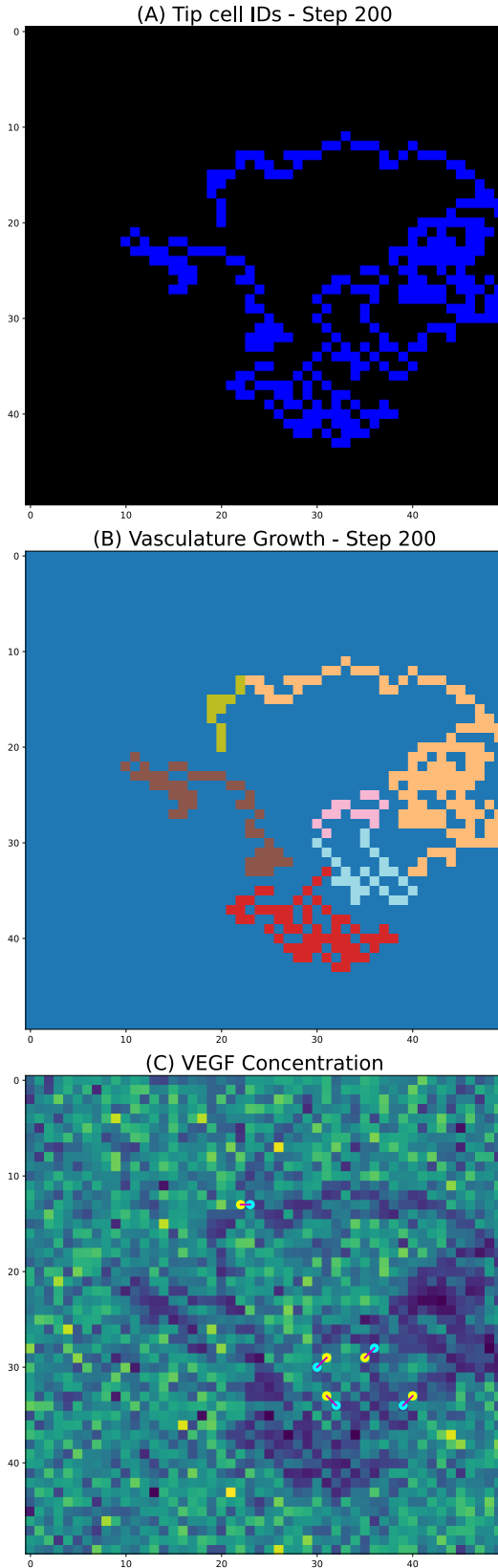


Figure 3.1.4: Step 200. Final state of angiogenesis simulation at Step 200, showing tip cell positions, vessel branching patterns, and the underlying VEGF concentration field.

The visualizations presented in Figure 3.1.4 provide comprehensive information on the behavior and outcomes of our computational angiogenesis model. Figure 3.1.4 (A) is a binary representation showing the complete vascular network formed after 200 simulation steps. The vessels are rendered in blue against a black background. The visualization reveals an intricate branching pattern with multiple pathways and junction points. Of particular note is the single remaining active tip, visible at the periphery of the network (marked with ‘1’), which represents the only remaining growth point in the system. Figure 3.1.4 (B) is a color coded map that assigns distinct colors to each of the six initially seeded vessel tips, allowing identification of their growth trajectories throughout the simulation. Visualization enables tracking of individual vessel paths, their interactions, and their terminal positions. The differentiated coloring reveals how some vessels achieved greater spatial coverage, while others remained more localized or merged with neighboring vessels. Figure 3.1.4 (C) is a heat map that illustrates the spatial distribution of VEGF across the 50×50 grid at simulation completion. Brighter yellow-green areas indicate higher concentrations of VEGF, while darker blue regions represent lower concentrations. The heterogeneous distribution patterns demonstrate the complex chemotactic environment navigated by the growing vessels throughout the simulation.

In this simulation step, we observe the growth behavior of a single tip of a vessel (ID 1) (Figure 3.1.4) that navigates through a VEGF. The tip of the vessel begins at position (32, 41) with a relatively low VEGF value of 0.0272. Based on its previous direction of movement from position (31, 42), the algorithm identifies five potential neighbor positions that maintain directional consistency. After evaluating the VEGF concentration at each valid neighboring position, the highest concentration of 0.028456 is found at position (33, 41), making this the next position in the vessel’s growth path. Once at this intermediate position, the algorithm recalculates the vessel’s movement direction and generates a new set of forward-bias neighbors. From position (33, 41), the vessel eventually grows to position (33, 40) with a VEGF value of 0.0246. This demonstrates how the vessel growth algorithm makes sequential decisions by following the VEGF gradient while maintaining reasonable directional continuity from its previous movement path.

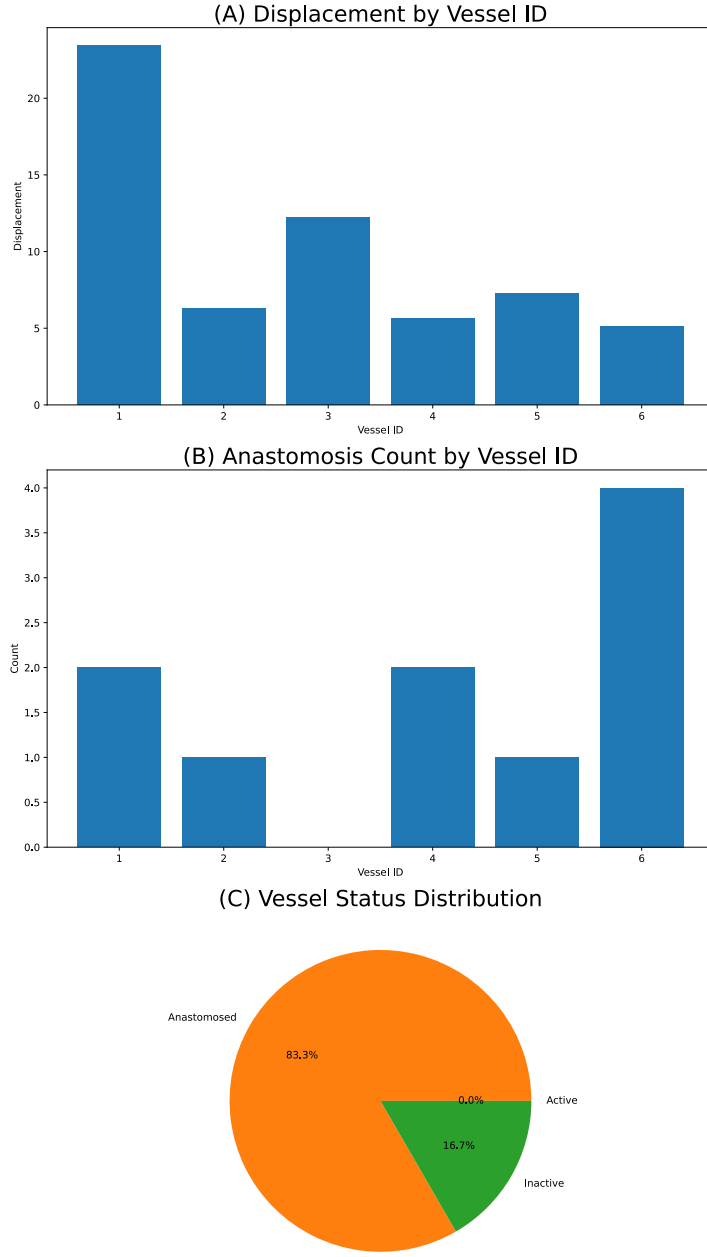


Figure 3.1.5: A complete vasculature network formed by the end of the simulation, illustrating vessel branching and overall growth patterns.

At the end of the simulation, all tips underwent anastomosis or became inactive, with a total of five anastomosis events recorded. Vessel ID 1 demonstrated the greatest displacement (23.43 units) (Figure 3.1.5 (A)) and participated in two anastomosis events (Figure 3.1.5 (B)), indicating both extensive migration and successful network integration. Vessel ID 2 achieved a

displacement of 6.32 units and an anastomosis event, while Vessel ID 3 displaced 12.21 units but became inactive without participating in any anastomosis, suggesting isolated growth. Vessel IDs 4 and 5 recorded displacements of 5.66 and 7.28 units, respectively, each completing one to two anastomosis events, supporting their contribution to network connectivity. Vessel ID 6 showed the shortest displacement (5.10 units) but engaged in the highest number of anastomosis events (four), highlighting its key role in the formation of vascular loops. Collectively, the final configuration reflects the successful maturation of the network characterized by high anastomosis activity and diverse vessel growth patterns.

3.2 ECM-only Model

To investigate how the density of the extracellular matrix (ECM) influences vessel growth, three distinct gradient structures of the ECM were implemented: uniform, radial, and linear. The uniform gradient maintains a constant density of ECM throughout the entire grid, serving as a control condition to isolate the effects of heterogeneity in ECM. The radial gradient features an ECM density that changes concentrically outward from a central point, mimicking environments such as tumor cores where ECM properties radiate from a localized source. In the linear gradient, the density of ECM gradually varies along a single axis, creating a directional bias that can guide the migration of tip cells. By comparing vessel behaviors across these types of gradients, we can systematically assess how structural differences in the microenvironment affect angiogenic patterns and dynamics.

3.2.1 Uniform Gradient

This section observes the migration patterns of multiple endothelial tip cells within a uniform extracellular matrix (ECM) environment. The visualization depicts six distinct tip cells (Cell IDs 0-5) traversing through an ECM with a consistent density of 0.5000, represented by the teal background coloration.

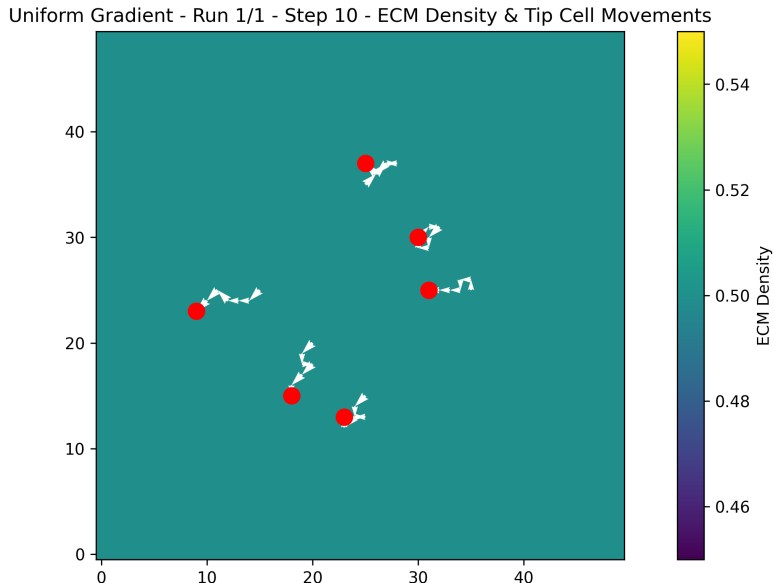


Figure 3.2.1: Initial positions of tip cells in a uniform ECM density environment at Step 0, showing six red cells with small directional indicators and consistent ECM density (approximately 0.50) throughout the simulation domain.

The temporal progression of tip cell migration within a uniform ECM environment demonstrates striking developmental patterns. In Step 0 (Figure 3.2.1), we observed six red tip cells positioned across the domain with minimal directional indicators, representing the initial state before migration.

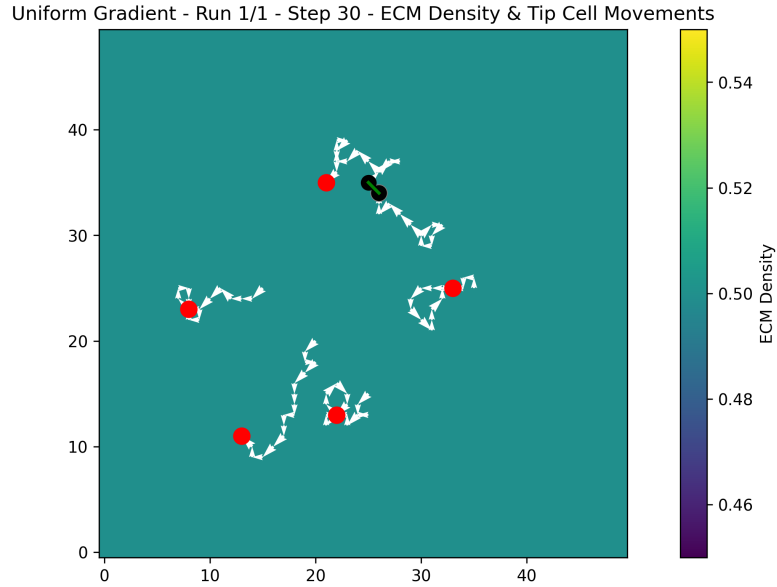


Figure 3.2.2: Tip cell migration patterns at Step 30, showing the development of branching white trajectories originating from red cells, with a black cell appearing in the upper portion of the domain indicating anastomosis event.

In Step 30 (Figure 3.2.2), these cells have begun establishing distinct migration pathways, as evidenced by the emergence of branching white trajectories emanating from each cell, with one cell transitioning to a black state, indicating anastomosis.

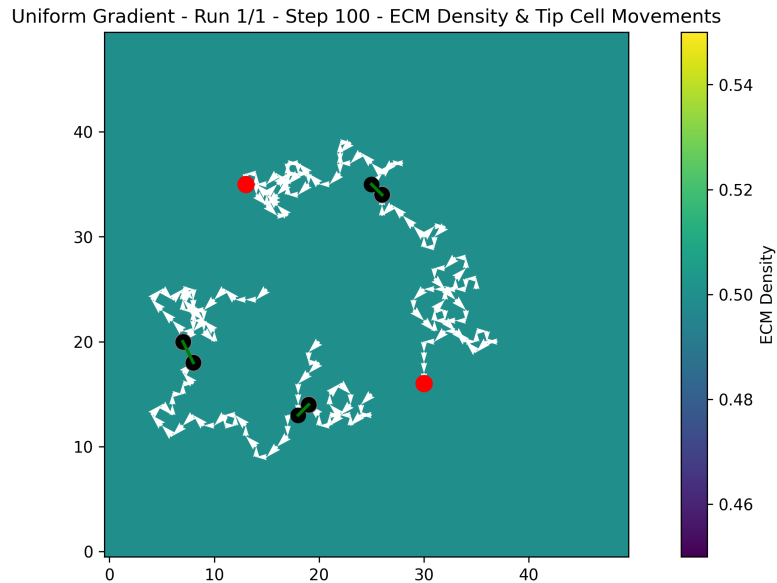


Figure 3.2.3: Advanced cell migration at Step 100, displaying more complex and extended trajectory patterns. Several red tip cells have transitioned to black cells, indicating blood vessels as migration progresses.

Upon progression to Step 100 (Figure 3.2.3), the migration tracks extend substantially and form more complex branching patterns, with additional cells converting from red to black, suggesting continued anastomosis events or cell state transitions.

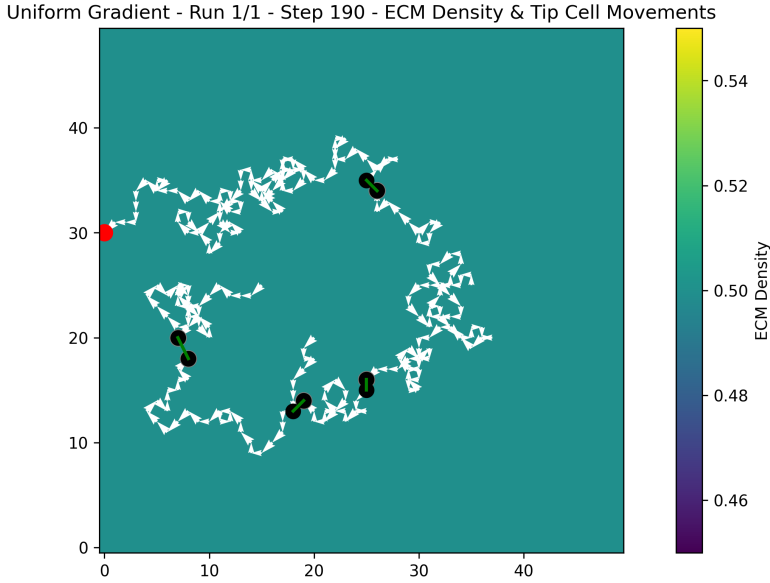


Figure 3.2.4: Extensive cell migration networks at Step 190, showing fully developed branching patterns. Most red cells have converted to black cells, with only one red cell remaining at the left edge of the domain. The white trajectories form an interconnected migration network across the simulation area.

In the final stage at step 190 (Figure 3.2.4), fully developed cellular networks with extensive branching structures that extended throughout the simulation domain were observed. Most cells have become black, with only one red cell remaining at the leftmost boundary. Throughout this progression, cells maintain their exploratory behavior within the consistent ECM density of 0.50, indicating that the observed migration patterns and cell state transitions occur independently of the influence of the ECM gradient.

The displacement metrics varied considerably between cells, with Cell 3 showing the highest displacement value (25.50), suggesting greater exploratory capacity, while Cell 5 showed the most limited movement (5.66). In particular, five out of six cells experienced anastomosis events (anastomosis count = 1), indicating cellular interaction or fusion with neighboring cells, while Cell 3 remained independent throughout the simulation period. This pattern of differential migration in a uniform gradient environment suggests that intrinsic cellular properties, rather

than ECM heterogeneity, may be the primary driver of observed variations in migratory behavior. The transition from red to black cell representation in the later time steps (as seen in the visual data from Figures 3.2.1, 3.2.2, 3.2.3, and 3.2.4) probably represents changes following anastomosis events, further supporting the dynamic nature of these cellular interactions.

3.2.2 Radial Gradient

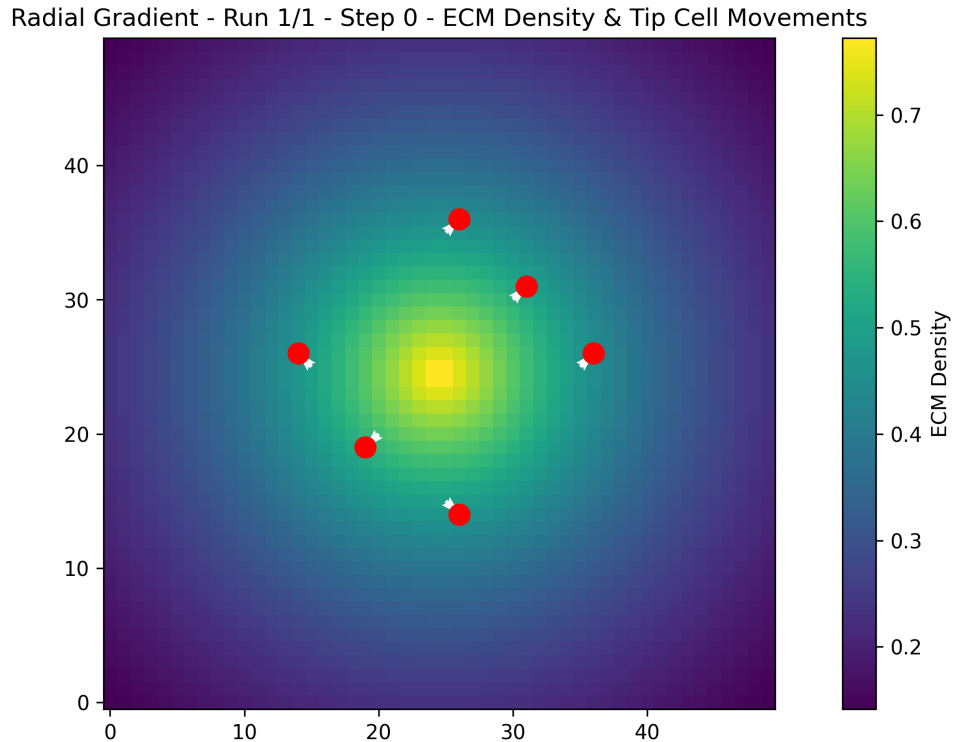


Figure 3.2.5: Radial gradient of ECM density at step 0 of the simulation. The initial positions of six red tip cells are distributed around the central high-density region. The white arrows indicate minimal initial movement vectors.

Figure 3.2.5 visualizes the initial step (Step 0) of a simulation showing the positions of the tip cells (in red) over a radial density gradient of the ECM (extracellular matrix), where the density of ECM is highest in the center (yellow) and decreases outward (purple). The white arrows indicate the initial movement direction of each tip cell. The simulation begins with seven tip cells, symmetrically distributed around the center, allowing the model to analyze how cells migrate in response to ECM cues under a radial gradient. This setup is critical for evaluating vessel sprouting behavior in tumor-induced angiogenesis.

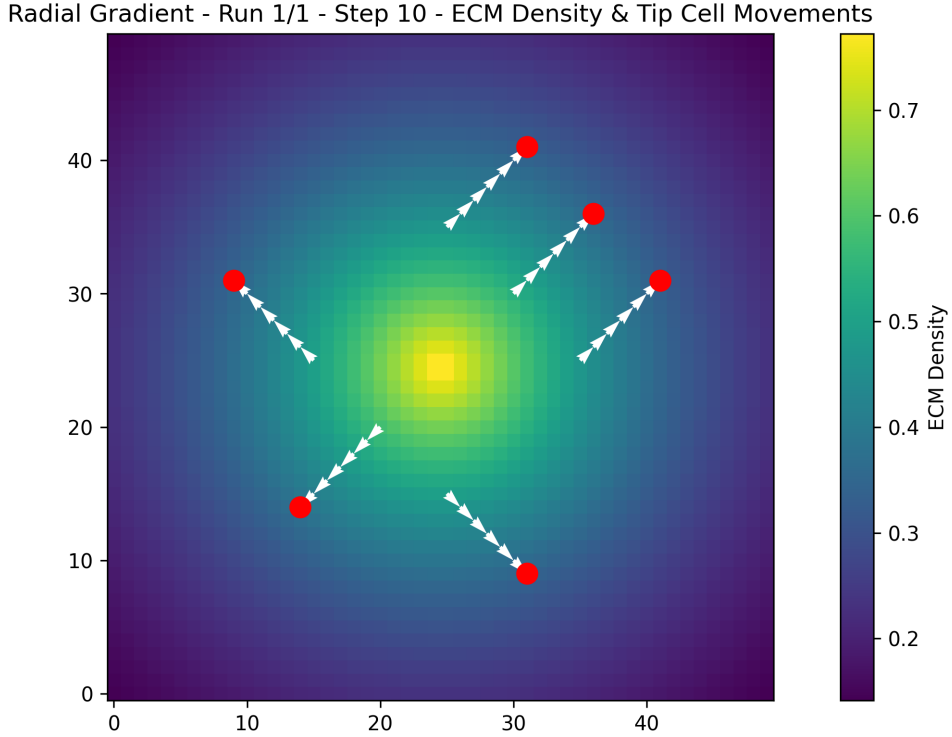


Figure 3.2.6: Radial gradient of ECM density at steps 10 of the simulation. The white arrows now show more significant movement vectors, with all cells moving away from the high-density center region toward areas of lower ECM density.

The visualization in Figure 3.2.6 shows tip cells (represented by red dots) moving along white vector arrows, with a clear tendency to migrate toward areas of higher ECM density (indicated by the yellow-green center region with density values approaching 0.7), demonstrating chemotactic behavior in response to the ECM gradient. Cells placed on the periphery in lower density regions (purple areas with values around 0.2-0.3) appear to be moving directionally toward the central region of higher ECM concentration, suggesting that ECM density gradients may serve as important guidance cues for cellular migration in this experimental system.

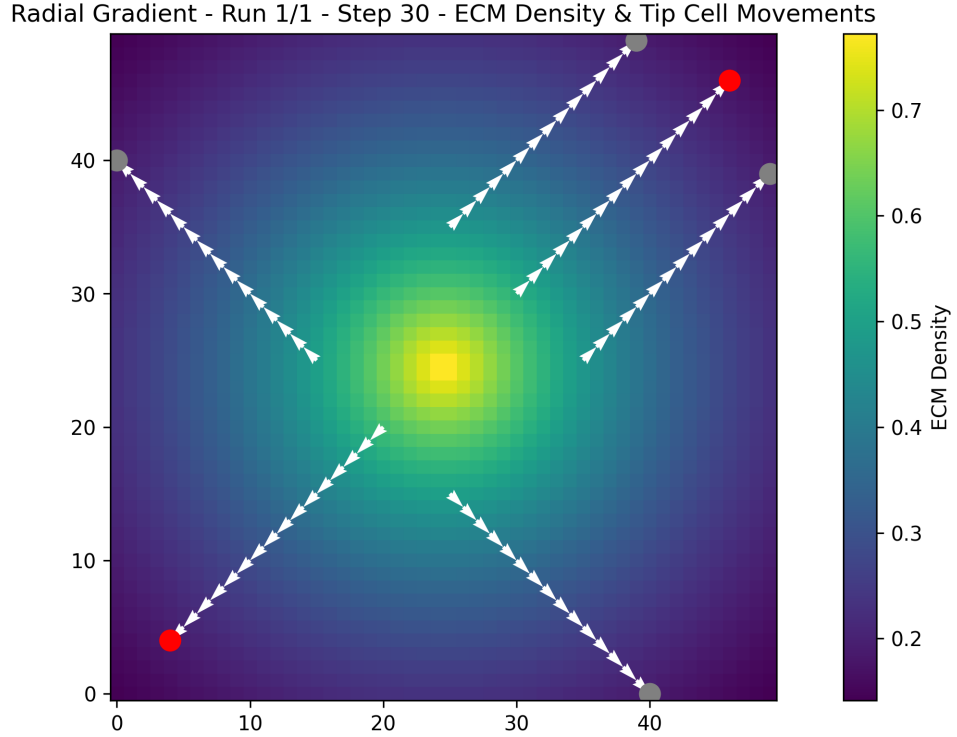


Figure 3.2.7: After 30 steps, most cells have moved to the periphery of the field. Five are now shown as gray dots, with one remaining red. The arrows show the complete movement trajectories of each cell from their starting positions.

The three images in Figure 3.2.5, 3.2.6, and 3.2.7 show a radial gradient of ECM density at different time steps (0, 10, and 30) of a simulation. The gradient is represented by a color map that varies from dark purple (low density ≈ 0.15) to bright yellow (high density ≈ 0.75), with the highest density in the center of the field (coordinates $\approx 25, 25$) and decreases outward. The heatmap, overlaid with white arrows, visualizes the trajectories of multiple cell tip-tops starting from a central origin point (marked in red) and moving toward peripheral regions (gray dots). Across all directions, tip cells move away from the center, suggesting that cells are repelled by higher ECM density zones or are migrating along other influencing cues.

Each cell follows a specific trajectory from areas of higher ECM density toward areas of lower density. CellID 0, the ECM value decreases from 0.4707 at position (14, 26) to 0.1877 at (0, 40). A similar decline pattern is observed for the other cells. The variance in displacement suggests that not all cells respond identically to the matrix conditions. Cells with higher displacement

(CellIDs 4 and 5) might be more efficient at overcoming adhesion forces or more sensitive to the ECM gradient. With zero anastomosis counts in all cells, the experimental conditions likely did not favor cell-cell fusion or network formation. This might be expected in experiments designed to assess purely individual migration rather than collective behavior. This is because the gradient design allows one to pick the lowest ECM value for the next position of the tip cell, which is the furthest point from any given point, and therefore the randomness did not affect the system. Cell ID 1 traveled along the longest path, displacements of 12.68 units, and cell ID 6 traveled the shortest path with a displacement of 4.24 units, moved through a wider range of ECM densities compared to other cells, suggesting possible adaptation to varying matrix conditions.

3.2.3 Linear Gradient

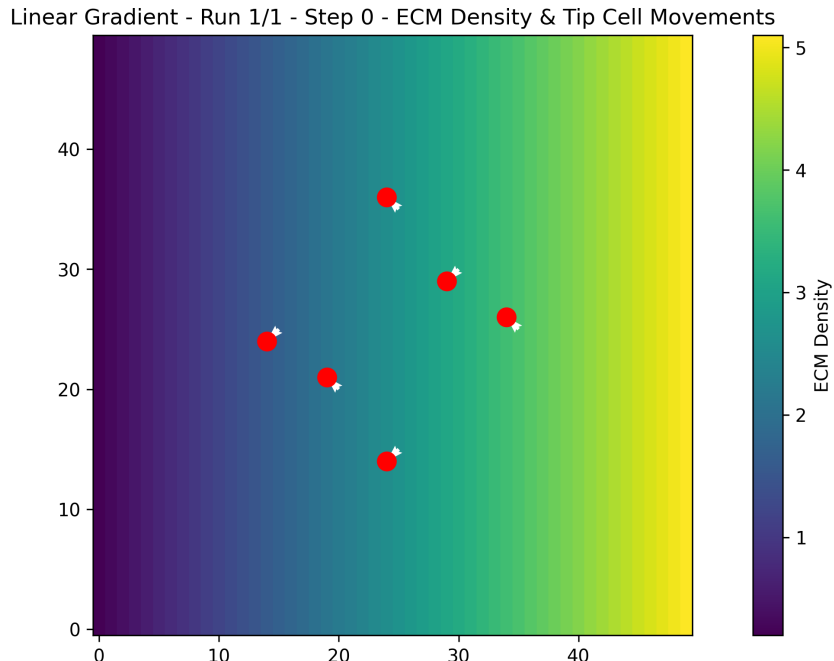


Figure 3.2.8: Linear Gradient - Run 1/1 - Step 0 - ECM Density & Tip Cell Movements. Initial positioning of six tip cells (red dots) across a linear ECM density gradient, with density increasing from left (purple/blue, low density) to right (yellow, high density). Small white arrows indicate the initial direction of movement for each cell. The color bar indicates ECM density values ranging from approximately 0 to 5.

For this gradient, Figure 3.2.8 shows a left-to-right gradient of increasing ECM density, represented by the color spectrum that transitions from deep purple (~ 0 density) to bright yellow (~ 5 density). Within this gradient, see Figure 3.2.8, the white arrow trajectories illustrate that the tip cells predominantly navigate through lower density regions (purple to teal, density values 0.2-3.6) while generally avoiding the high density zones (green to yellow, density values > 3.6).

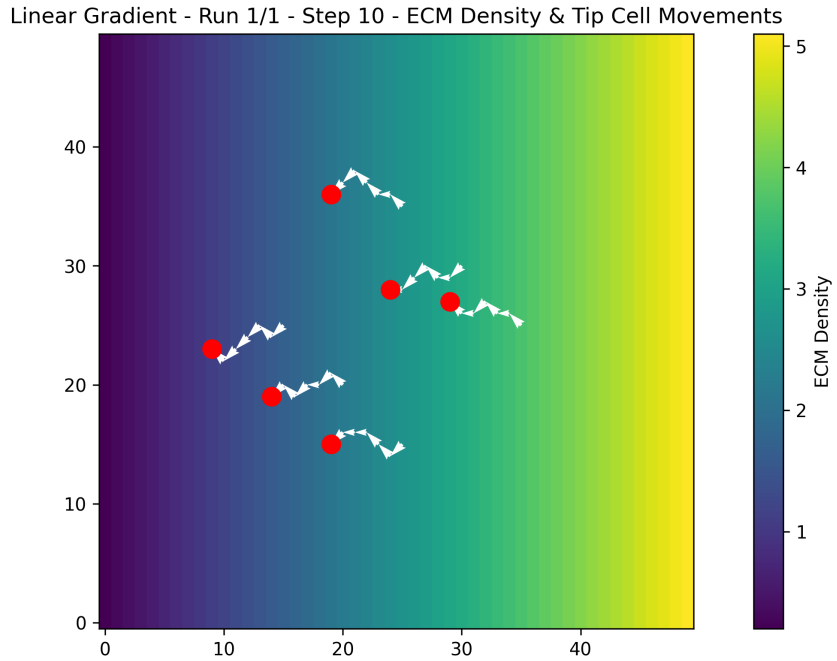


Figure 3.2.9: Linear Gradient - Run 1/1 - Step 10 - ECM Density & Tip Cell Movements. Progression of six tip cells (red dots) after 10 simulation steps, showing their movement trajectories (white arrows) through the ECM density gradient.

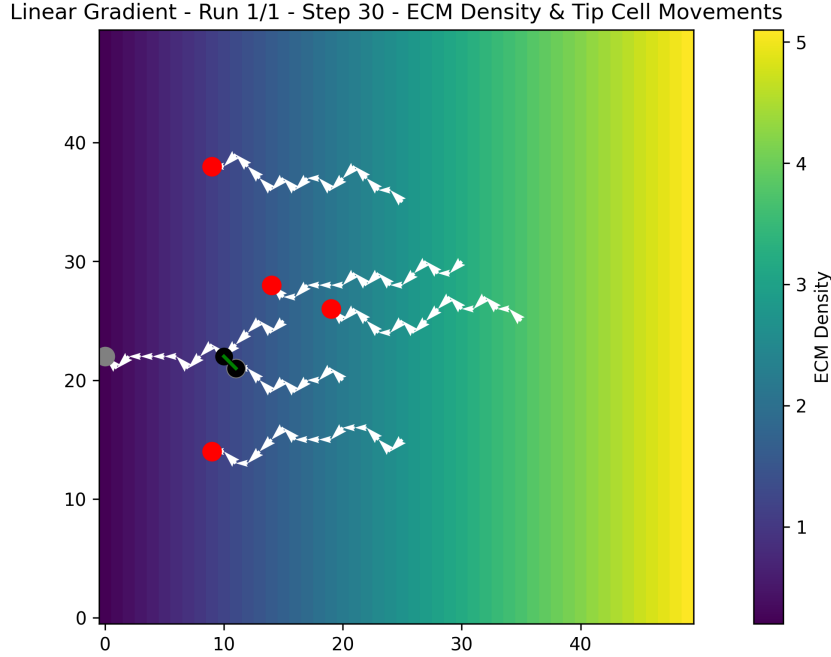


Figure 3.2.10: Linear Gradient - Run 1/1 - Step 30 - ECM Density & Tip Cell Movements. Advanced stage of cell migration after 30 simulation steps, showing five tip cells (four red dots and one black dot with green outline) with extended movement trajectories (white arrows).

The distribution of the cell paths suggests a complex interplay between contact guidance and haptotaxis, as evidenced by the characteristic zigzag movement patterns that align with local density variations. The circular black markers along specific cell paths indicated anastomosis events (Figure 3.2.10) that appear due to their proximity. The randomly chosen positions are among the lowest density values, suggesting that these regions may create favorable microenvironments for the recognition and fusion of cell-cell interactions. Furthermore, the distribution of trajectories in various vertical positions $Y \approx 14 - 38$ indicated a substantial exploration of the available space, with cell 3 achieving the most extensive vertical range compared to the more horizontally restricted paths of cells 2 and 4. These visual data strongly support the quantitative findings that ECM density gradients influence both directional persistence and the probability of tip cell anastomosis.

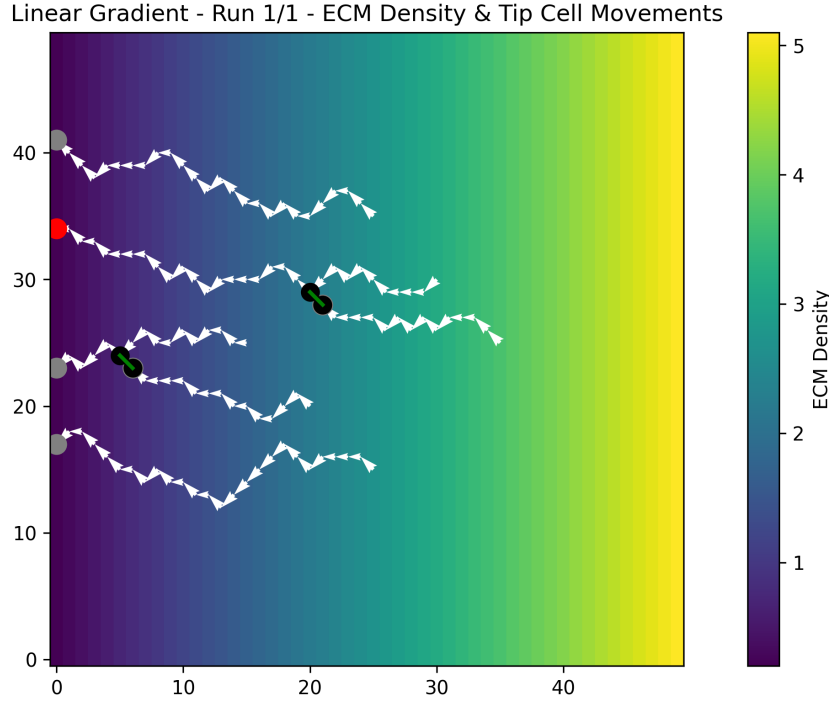


Figure 3.2.11: Linear Gradient - Run 1/1 - ECM Density & Tip Cell Movements. Final state of the simulation showing the complete migration paths of multiple cells through the ECM density gradient. Several gray dots on the left side and one red dot in the upper-left quadrant represent the final cell positions, while two black dots with green outlines indicate cells that have anastomosed. Grey has become inactive, and red is still active. The white arrow trajectories demonstrate the full migration history, revealing a general trend of movement from low-density regions (left) toward higher-density regions (right). The color bar indicates ECM density values ranging from approximately 0 to 5.

As illustrated in Figure 3.2.11, cells predominantly traversed regions of higher ECM density (3.6-0.2), exhibiting characteristic trajectories with frequent directional adjustments. From the analysis of the data set, we found that cells with greater total displacement (specifically cells 2, 3, and 5, covering 25.02, 25.02, and 30.59 units, respectively) demonstrated an enhanced capacity to navigate through intermediate-density matrices while maintaining overall directional persistence toward lower-density regions. Anastomosis events were observed exclusively in cells 1 and 4, occurring at specific ECM density thresholds (range: 3.6-1.3), suggesting that cell-cell connections may be density dependent. Furthermore, vertical exploration varied considerably between cell populations, with cells 0 and 2 maintaining lower vertical positions $Y \approx 14 - 24$ compared to cell 3, which achieved the highest vertical exploration $Y \approx 36 - 39$. These findings collectively indicate that the migration dynamics of tip cells is modulated by ECM density gra-

dients as they navigate from regions of higher to lower matrix density. Cell 5 demonstrated both the greatest displacement and navigation in the ECM density range (3.1-0.2). These observations have implications for understanding the formation of the vascular network in heterogeneous tissue environments, particularly how endothelial tip cells respond to mechanical signals during angiogenesis.

3.2.4 Mean Displacements

We ran simulations of uniform, radial and linear gradients 20 times to collect data on the displacements of tip cells in each run or simulation. We combined the mean displacement values for each gradient type from 20 runs and performed one-way ANOVA on the data to determine whether the mean displacement of the tip cells differs significantly between the three gradient types. Each gradient condition was simulated 20 times to ensure statistical robustness, and the mean displacement of tip cells was measured in all simulations.

Null Hypothesis (H_0): The mean displacement of the tip cells does not differ between the three gradient types (uniform, radial and linear). Mathematically expressed as: $\mu_1 = \mu_2 = \mu_3$, where μ represents the mean displacement for each gradient type.

Alternative Hypothesis (H_1): The mean displacement of the tip cells differs between at least two of the three gradient types (uniform, radial and linear). Mathematically expressed as: at least one $\mu_i \neq \mu_j$ for $i \neq j$.

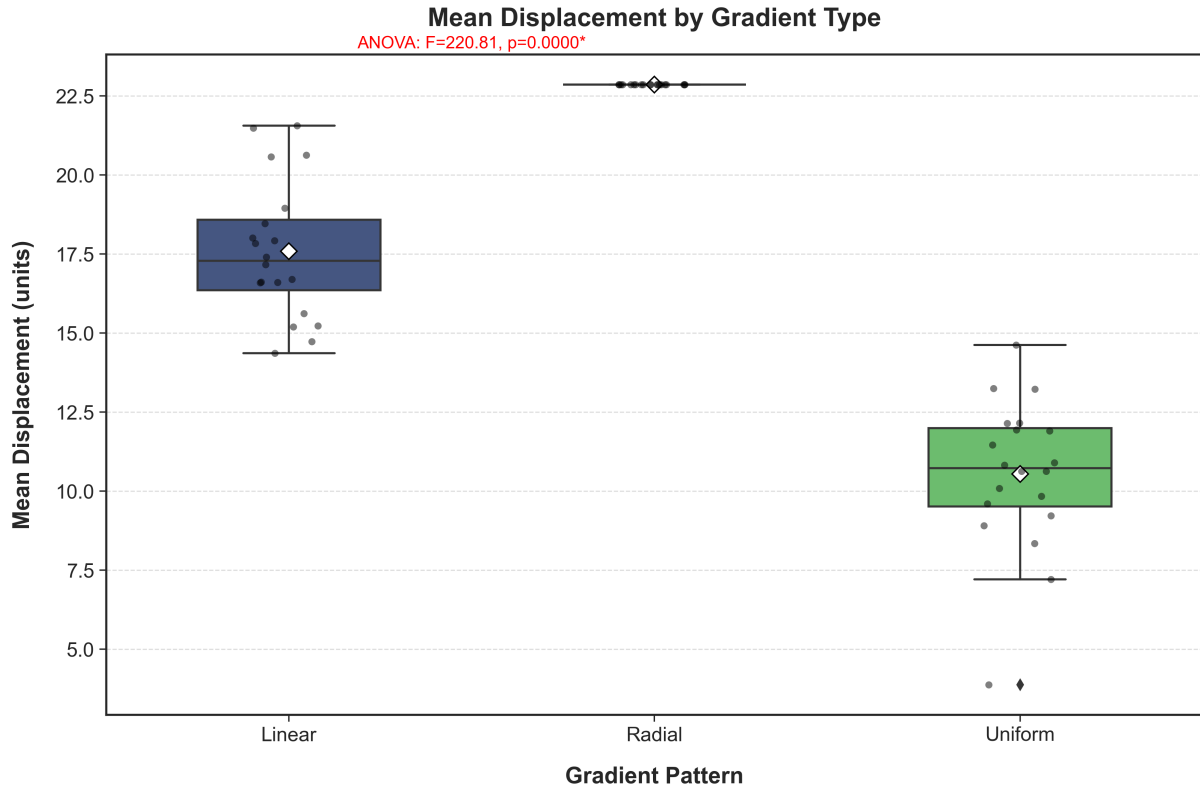


Figure 3.2.12: The one-way ANOVA analysis yielded a highly significant result with $F = 220.81$ and $p < 0.0001$, strongly indicating that the gradient type has a substantial effect on cellular displacement.

The analysis yielded an F-statistic of 220.81 with a corresponding p value of 1.43×10^{-27} , indicating an extremely significant effect of gradient type on cell displacement (Figure 3.2.12). This provides statistical evidence to reject the null hypothesis(H_0). Figure 3.2.12 visually reinforced the statistical findings by showing all individual data points from the 20 simulation runs for each gradient type. The linear gradient displayed a greater vertical spread (approximately 14.5-21.5 units), revealing greater variability in cellular displacement. In the radial gradient, points cluster tightly around 22.5 units with minimal variation, indicating highly consistent cellular responses across simulations. The uniform gradient showed the widest relative distribution, with most values between 7.5-13 units and a notable outlier at approximately 4 units. The clear separation between these three non-overlapping distributions visually confirmed the robust statistical differences ($F = 220.81$, $p < 0.0001$) found in the ANOVA analysis, providing

compelling evidence that the gradient pattern significantly influences the migration behavior of the tip cells.

The Tukey Honestly Significant Difference (HSD) test is conducted to evaluate pairwise differences in mean displacement between three different ECM gradient structures: uniform, radial and linear. The test controls the family-wise error rate (FWER) at an alpha level of 0.05. For each pair of gradient types, the hypotheses are as follows:

Null Hypothesis (H_0): The mean displacement between the two groups is equal.

$$\text{Group 1} = \text{Group 2}$$

Alternative Hypothesis (H_1): The mean displacement between the two groups is not equal.

$$\text{Group 1} \neq \text{Group 2}$$

tukey_results						
group1	group2	meandiff	p-adj	lower	upper	reject
Linear	Radial	5.2794	0.0	3.8633	6.6955	TRUE
Linear	Uniform	-7.0452	0.0	-8.4613	-5.629	TRUE
Radial	Uniform	-12.3246	0.0	-13.7407	-10.9085	TRUE

Figure 3.2.13: Post-hoc Tukey HSD pairwise comparison results of mean displacement across different gradient types.

The Tukey HSD test confirmed that the radial gradient produced a significantly higher mean displacement than the linear gradient, with a mean difference of 5.28 units (95% CI: 3.86 to 6.70) (Figure 3.2.13). This substantial positive difference indicates that the central signal pattern emanating from the radial gradient is significantly more effective in promoting cellular displacement than the directional signals provided by the linear gradient. Comparison between the linear and uniform gradients revealed that the linear gradient yielded significantly greater displacement, with a mean difference of 7.05 units.

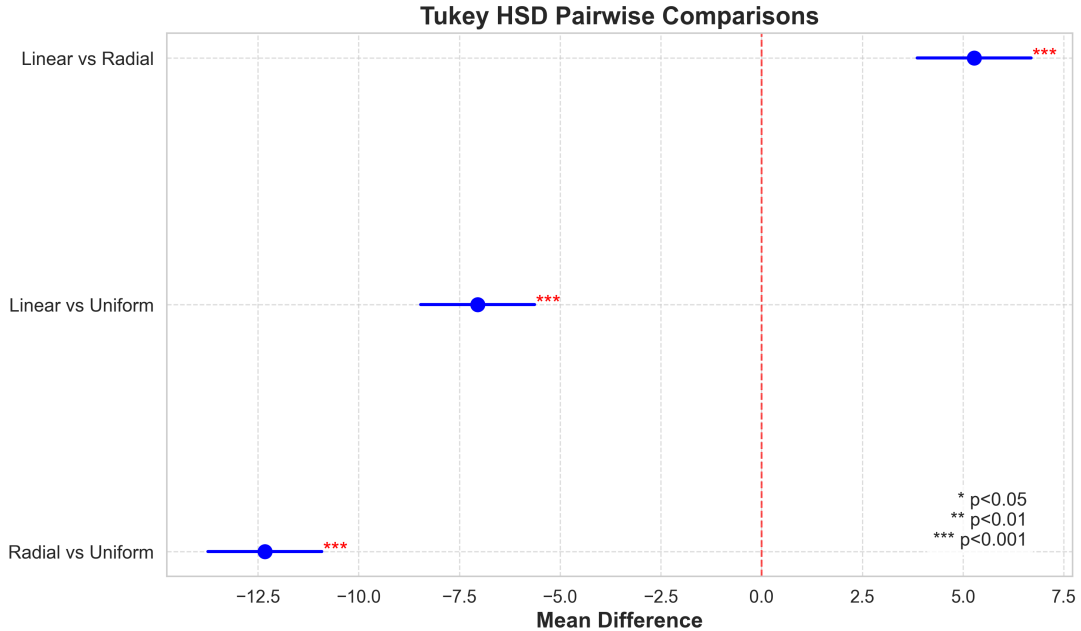


Figure 3.2.14: Following the highly significant ANOVA results ($F = 220.81, p < 0.0001$), the post-hoc analysis revealed statistically significant differences between all paired comparisons ($p < 0.001$ for all pairs).

In Figure 3.2.14, because the adjusted p-values are all < 0.001 , we reject the null hypothesis (H_0) in the three pairwise comparisons, confirming that each group is significantly different from the others. The mean difference represents the difference between the mean values of the two types of gradients compared in each row (Figure 3.2.14). The consistency of these significant differences across all pairwise comparisons, coupled with the non-overlapping confidence intervals, provides robust evidence for a clear hierarchical relationship in the effectiveness of different gradient patterns. This hierarchical relationship directly refers to the measured distance that cells travel, with radial gradient conditions producing the longest migration distances, followed by linear, and then uniform producing the shortest migration distances. These findings suggest that the spatial organization of gradient patterns plays a crucial role in determining the efficiency of cellular migration, with centrally organized patterns eliciting the strongest migratory response.

3.3 Merged (ECM and VEGF) Model

In this model, we have added the VEGF concentration as a parameter to the existing ECM-only model. Therefore, this model has VEGF concentration and ECM density factor that affects the role in the tip cell movement logic. We have changed the movement algorithm for a tip cell to account for the VEGF concentration and the density of the ECM when they decide to grow.

3.3.1 Uniform Gradient

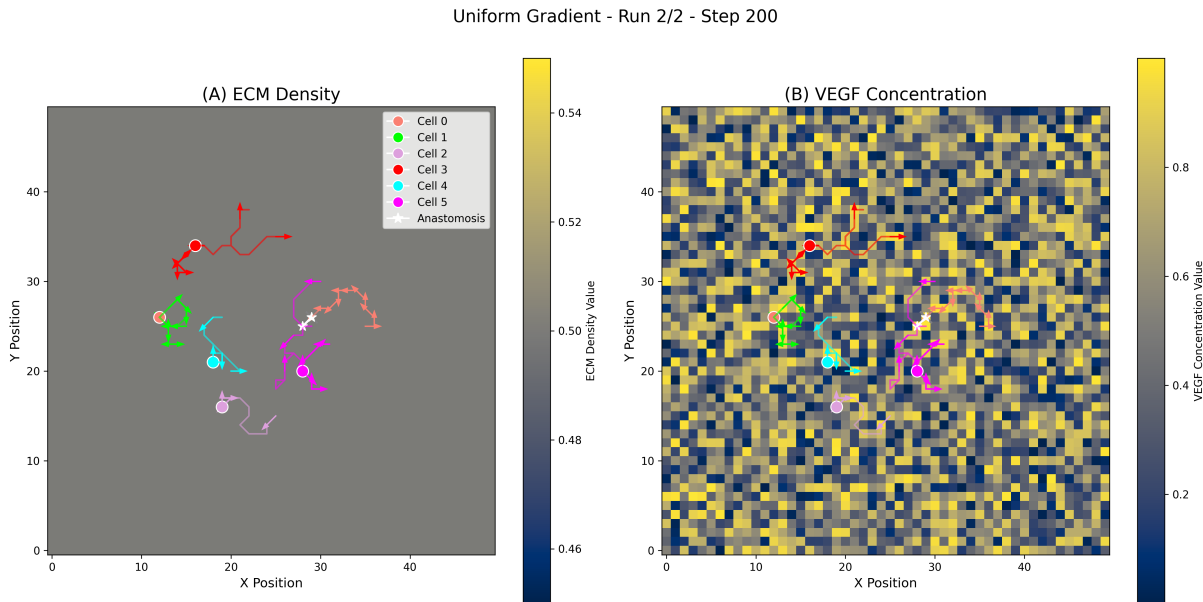


Figure 3.3.1: Cell Migration Patterns with ECM Density (uniform gradient) and VEGF Concentration

In this advanced stage simulation (step 200 of run 2/2), Figure 3.3.1 reveals a significant temporal evolution of the angiogenic process compared to earlier time points. Figure 3.3.1 (A) shows the cellular migration paths through a uniform ECM density field (0.46-0.54), while Figure 3.3.1 (B) displays the corresponding heterogeneous VEGF concentration field (0.2-0.9). Cellular trajectories have become notably more complex and extensive, with longer and more branched migration paths than in earlier steps, particularly evident in cells 0, 3, and 5. An anastomosis event (marked by white crosses) has occurred between cells 5 and 0, indicating a successful vessel connection, a critical milestone in angiogenesis. Cells appear to preferentially navigate regions

of higher concentrations of VEGF (yellow patches in Figure 3.3.1 (B)), while their paths show notable tortuosity and directional changes, suggesting an active chemotactic response despite the relatively uniform environment of the ECM. This temporal progression demonstrates how initially separated endothelial cells can form interconnected vascular networks over time through persistent migration and selective cell-cell interactions.

3.3.2 Radial Gradient

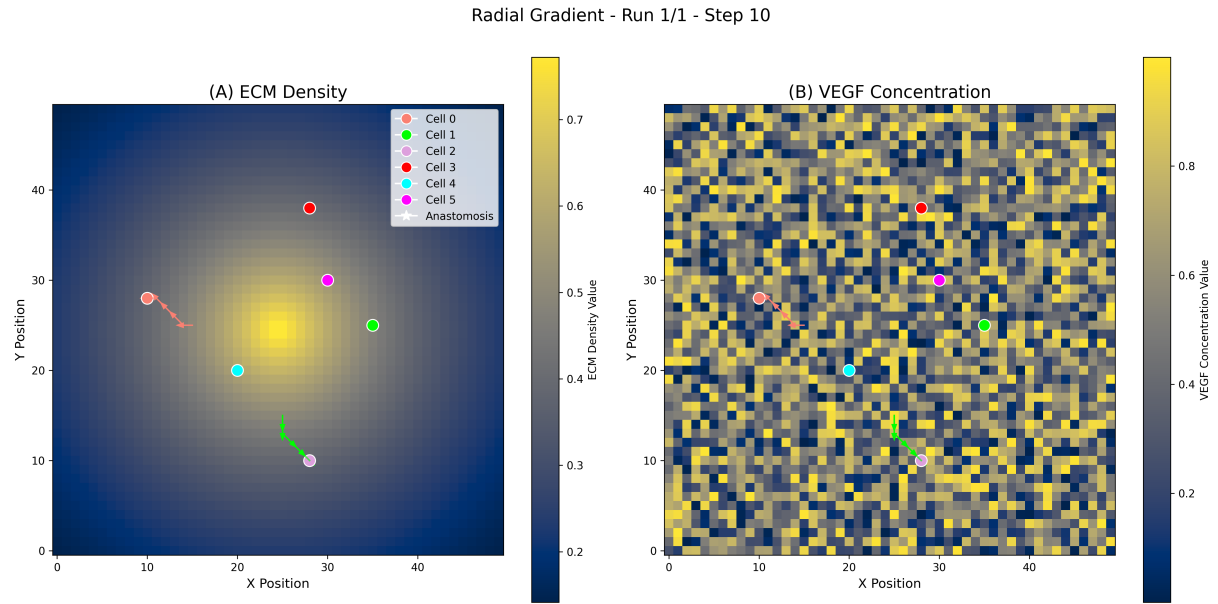


Figure 3.3.2: Cell Migration Patterns with ECM Density (radial gradient) and VEGF Concentration

In our simulation of the radial gradient, an inconsistency was observed in the movement of tip cells in Figure 3.3.2. Specifically, while the model initializes six tip cells, only two consistently exhibit movement, whereas the others remain stationary. This behavior contrasts with results obtained under uniform and linear gradient conditions, where all tip cells move as expected.

This discrepancy suggests that the radial gradient structure may create local symmetries or stagnation points that impede cellular migration. To address this issue, adding minor perturbations to the VEGF gradient can help break perfect symmetry and prevent cells from becoming trapped in static regions. Furthermore, the enforcement of a small baseline movement ensures that all cells undergo at least minor displacement, regardless of gradient differences. A stochas-

tic movement component could be introduced when gradient differences are insufficient to drive directional migration.

These modifications aim to improve robustness in cellular movement and ensure that the model accurately reflects expected biological behaviors across different gradient conditions. Future refinements will focus on optimizing these adjustments while maintaining physiological relevance.

3.3.3 Linear Gradient

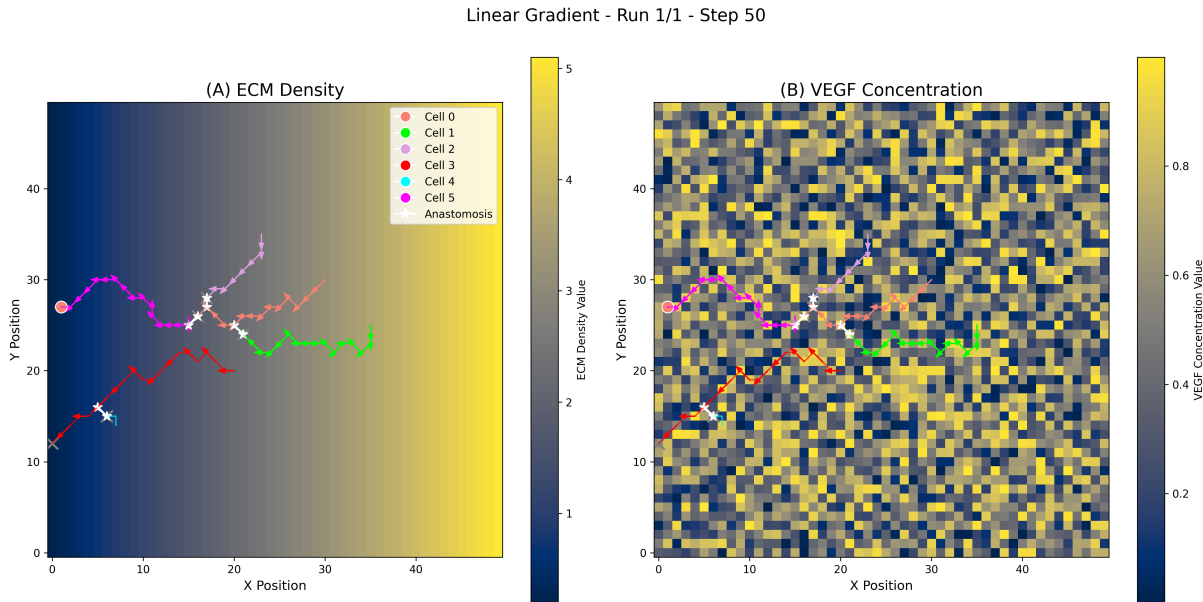


Figure 3.3.3: Cell Migration Patterns with ECM Density (linear gradient) and VEGF Concentration

This linear gradient simulation (Run 1/1, Step 50) reveals a striking contrast to the uniform gradient models previously examined. Figure 3.3.3 (A) shows a pronounced left-to-right ECM density gradient (ranging from approximately 0.5 to 5.0), which appears to strongly influence cell migration behavior. In particular, cells exhibit a clear directional bias toward regions of higher ECM density (yellow area), with trajectories predominantly moving rightward despite some tortuous paths. Multiple anastomosis events (marked by white crosses) have already occurred between cells 3, 5, 2, and 0, suggesting accelerated network formation compared to uniform gradient conditions. Figure 3.3.3 (B) shows that while the heterogeneous VEGF concentration field (0.2-0.9) introduces local variability in migration paths, the dominant ECM gradient appears to

be the dominant directional signal. This is evidenced by persistent rightward movement of cells despite the heterogeneity of VEGF, indicating that steep ECM gradients can override or work synergistically with VEGF chemotaxis to improve directed angiogenic sprouting and accelerate vessel network formation.

3.3.4 Comparison between ECM-only Model and Merged Model

To evaluate the effect of VEGF in conjunction with ECM gradients on tip cell displacement, we analyzed data from two models: the ECM-only model and the Merged model (ECM and VEGF). Displacement values were recorded across three gradient types, Linear, Radial, and Uniform, over multiple simulation runs. Summary statistics and inferential analyzes were conducted to assess differences in displacement behavior between the two conditions.

A t-test is used to determine whether there is a statistically significant difference between the displacement values of two models under different gradient types (linear, radial and uniform).

Null Hypothesis (H_0): There is no significant difference in displacement values between the ECM-only and Merged models.

Alternative Hypothesis (H_1): There is a significant difference in displacement values between the ECM-only and Merged models.

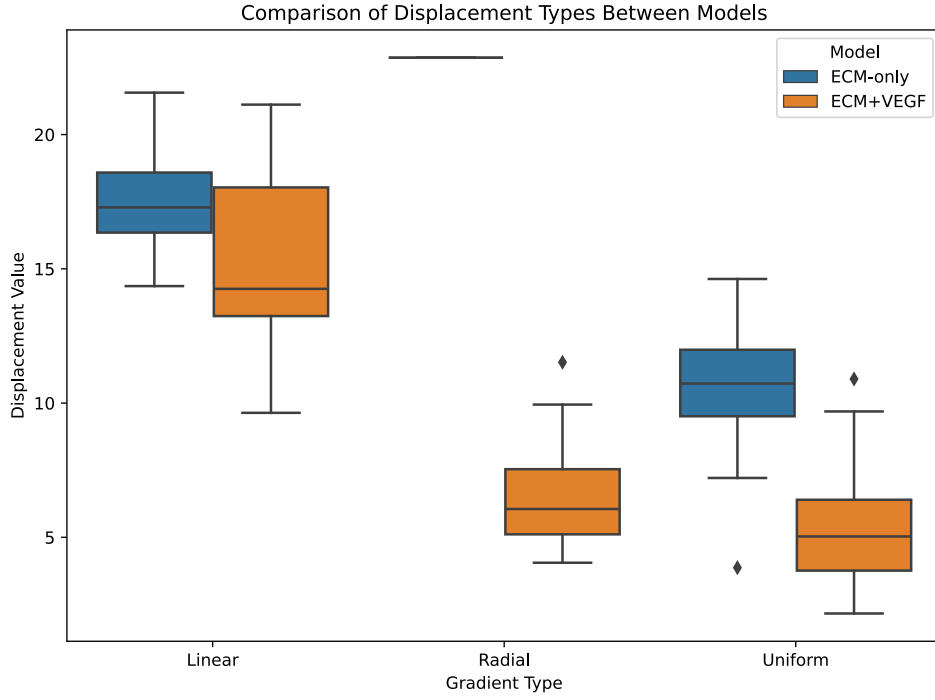


Figure 3.3.4: Box plot analysis of displacement magnitude across three gradient patterns in ECM-only and the Merged models.

Figure 3.3.4 illustrates the distribution of displacement values in the ECM-only (blue) and ECM and VEGF (orange) models in linear, radial and uniform gradient types. Black diamonds indicate potential outliers, and the horizontal line above the radial category signifies statistical significance between the two conditions.

The radial gradient has the highest t statistic ($t = 39.13$) and an extremely low p-value ($p = 1.25 \times 10^{-19} < 0.05$), confirming a strong and statistically significant difference in displacement between models. The linear gradient has a moderate t-statistic ($t = 2.32$) and a p-value ($p = 0.027 < 0.05$), indicating a significant but smaller difference. Similarly, the uniform gradient exhibits a statistically significant difference ($t = 6.80, p = 4.56 \times 10^{-8} < 0.05$). The displacement analysis indicates that the ECM-only model consistently yields higher displacement values than the Merged (ECM and VEGF) model, with a particularly strong divergence under the radial gradient condition. The statistical significance of these results suggests that the presence of VEGF influences displacement dynamics differently between gradient types.

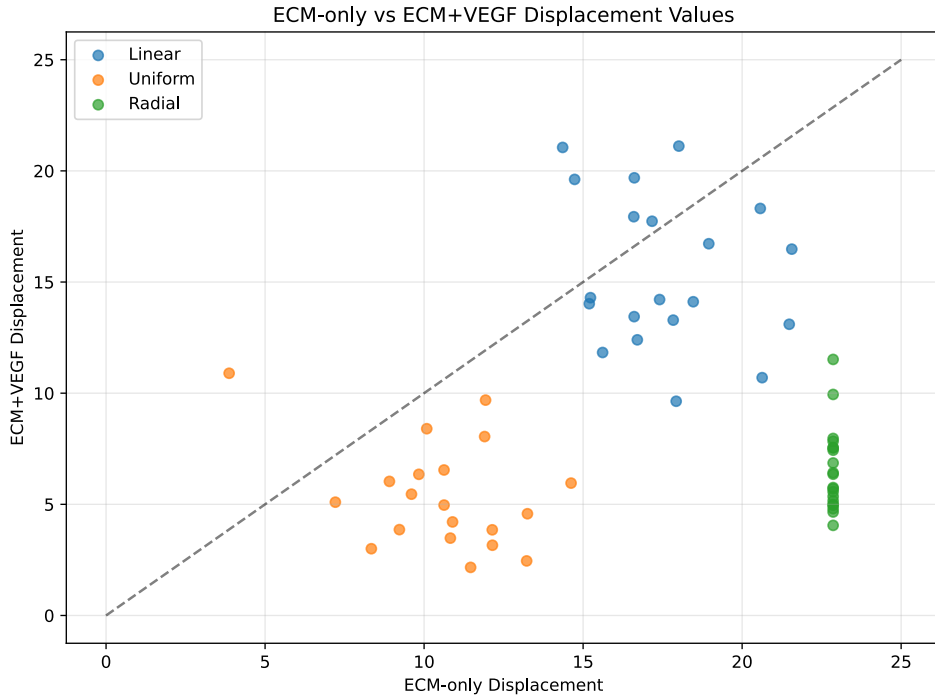


Figure 3.3.5: Comparative scatter plot of corresponding displacement measurements between model conditions.

Figure 3.3.5 presents a direct comparison of displacement values between conditions, only with the ECM (x-axis) and the merged model (ECM and VEGF) (y-axis) for each displacement type (linear blue, uniform orange and radial green). Points falling below the dashed equality line ($y=x$) represent instances where VEGF addition resulted in reduced displacement. The visualization reveals that while linear displacement shows variable effects with some points approaching the equality line, both radial and uniform displacements consistently demonstrate suppression in the presence of VEGF, with radial displacement exhibiting the most consistent reduction across all measured values.

The results strongly support the alternative hypothesis (H_1) that VEGF significantly alters the displacement patterns of the ECM gradients. Therefore, we reject the null hypothesis (H_0). The scatter plot (Figure 3.3.5) clearly illustrates this effect, with nearly all data points falling below the identity line, particularly for radial and uniform gradient types. The box plot (Figure 3.3.4) further demonstrates the consistent pattern of reduced displacement in the presence of VEGF in all types of gradients, with distributions showing a distinct separation between conditions.

4

Discussions and Conclusions

The goal of this project was to improve a previous agent-based model of triple negative breast cancer [28, 29] by adding an ECM module to the model. The motivation behind the addition of this module was to establish a more realistic method to measure how ECM density influences vascular structure. The existing model measured the density of ECM as a static parameter without accounting for the dynamic remodeling that occurs during angiogenesis. By implementing a gradient-responsive migration algorithm, we can now observe how tip cells actively modify their microenvironment while simultaneously responding to changing density conditions.

The general finding is that the configuration of the gradient pattern significantly impacts the cellular displacement, with a clear hierarchy of effectiveness in the ECM-only model. Radial gradients produce the highest cell displacement (approximately 22.5 units), followed by linear gradients (approximately 17.5 units), with uniform gradients producing the lowest displacement (approximately 10.5 units). This relationship is statistically robust (ANOVA: $F=220.81$, $p < 0.0001$) with highly significant differences between all pairwise comparisons (Tukey HSD: $p < 0.001$ for all pairs). Substantial mean differences, particularly between radial and uniform gradients (12.32 units), demonstrate that the spatial organization of chemical signals fundamentally determines cellular migration efficiency, with centrally emanating patterns (Radial)

eliciting the strongest and most consistent directional response compared to directional (Linear) and nondirectional (Uniform) patterns.

Qutub et al. emphasize the critical role of growth factor gradient configurations in directing cellular migration, which aligns with our model ECM-only findings. Our design shows that radial gradients produce superior displacement compared to Linear and Uniform patterns, complementing their observation of the differential effects of ligand concentrations on directional persistence [34]. This study [14] also emphasizes the role of growth factors, particularly VEGF, in the direction of cellular migration and angiogenesis. The models discussed, such as those by Köhn-Luque et al. and van Oers et al., highlight how local accumulation of VEGF through ECM binding influences cell chemotaxis and migration patterns. Furthermore, the findings regarding the mechanics and configurations of the ECM support the idea that different properties of the ECM and the distributions of growth factors significantly affect cell behavior during angiogenesis [14]. The significant differences we found between different gradient configurations experimentally validate their systems biology model, which highlights previously unexplored interactions in angiogenesis. The statistical analysis of our model shows highly significant differences between gradient patterns, providing concrete data supporting the importance of understanding key cellular mechanisms that drive angiogenesis [34].

We compared the ECM-only model with the Merged model to observe the significance of VEGF with ECM gradients during tip cell migration in angiogenesis. Studies such as those by Daub et al. integrate both VEGF chemotaxis and ECM-guided haptotaxis to simulate endothelial cell migration during angiogenesis [11]. Their model demonstrates that the inclusion of VEGF gradients significantly enhances tip cell displacement compared to ECM-only conditions, which supports the findings of our analysis between the ECM-only model and the Merged model. From two-sample t-tests (Welch's t-test), we found that inclusion of VEGF leads to statistically significant increases in tip cell displacement in linear, radial, and uniform ECM gradient environments. Among the few reasons for this significance, Krishnan et al. mention how the properties of ECM, such as stiffness and composition, influence the behavior of endothelial cells during

angiogenesis [16]. The research indicates that VEGF not only serves as a chemotactic factor, but also modulates the remodeling of the ECM through matrix metalloproteinases (MMPs), facilitating increased tip cell migration. These insights corroborate our findings on the effects of VEGF and ECM gradients in promoting tip cell displacement.

4.1 Next steps

A long-term goal for this project would be to explore how matrix metalloproteinases (MMP) affect angiogenesis. MMPs degrade components of ECM such as collagen and elastin, clearing pathways for endothelial cells, and releasing growth factors such as VEGF to promote angiogenesis [12]. By breaking down ECM, MMPs reduce its density, facilitating new blood vessel growth in previously dense areas. MMPs also promote ECM stiffness through crosslinking with enzymes such as LOX, enhancing integrin signaling to increase cell migration and angiogenesis [5]. Building on the current model, which compares tip cell migration under various ECM gradient structures (linear, radial, and uniform) and evaluates the influence of VEGF gradients on cell displacement, the next step would be to incorporate MMP-mediated ECM remodeling. This would involve dynamically updating the density of the ECM in response to localized concentrations of MMP secreted by migrating tip cells. By simulating MMP secretion, diffusion, and decay, and linking ECM degradation and VEGF release to these dynamics, the model could capture a more realistic interaction between tip cells and their microenvironment. This enhancement would provide a framework for studying how MMPs modulate both physical barriers and biochemical signals during vascular morphogenesis.

In the next steps of developing this project, we would like to modify Merged model's radial gradient issue or a new design of a deterministic hybrid model of sprouting angiogenesis, similar to Milde et al., where their ECM model combines a vector field and a density field [23]. Their findings indicate that the migration direction of tip cells is determined by the fibronectin gradients (haptotaxis) and the VEGF gradients (chemotaxis), while the migration speed is de-

terminated by the fiber density of the ECM [23]. They found that the structure and density of the ECM had a direct effect on the morphology, expansion speed, and number of branches.

Some improvements that can be made to our designed model include the addition of VEGF gradients to the VEGF model. Qutub et al. developed a multiscale model of sprouting at the beginning of angiogenesis [33]. Although their model setup differs slightly from my model design, their simulations showed that the driving force of angiogenesis is a VEGF gradient rather than absolute VEGF concentrations [33]. We believe that adding VEGF gradients to our VEGF-only model would enhance comparability with the ECM model. Our designed model could also be improved by incorporating tip cell velocity and stalk cell proliferation, as [40] noted that these factors play an important role in the morphology of the vascular network.

4.2 Personal Reflection

Working on a senior project was a journey full of curiosity, learning, exploration, and problem solving. I started my senior year without knowing the fundamentals of cancer. Within a few months, I managed to learn about cancer in biology and deepen my understanding of cancer processes in the human body. It was the first time I had to teach myself a whole new area of biology independently. Although I was familiar with the agent-based computational approach, applying and mimicking the smallest details of cell movement in the angiogenesis process, how cells move, and what factors affect their movement, deepened my understanding of designing a model to make it more realistic.

Biology was not my favorite subject when I was in high school. This project marks a full-circle moment for me to overcome a small portion of the biology field and to enjoy learning about it. I have become familiar with MATLAB for plotting, combining my skills in biology and computer science. During the past eight months, I spent every week understanding the concept of cancer as I designed the next steps of the project, setting weekly goals, reassessing progress, and maintaining perspective on the big picture. Of course, I ran out of time and did not fully achieve the desired result of the Merged model; only preliminary result had been found.

Now, I feel confident in my ability to work in major scientific fields using agent-based modeling (ABM) through analytical, numerical, and theoretical approaches. I have gained valuable knowledge on cancer, the vascular system, agent-based modeling, and MATLAB. It is incredible to see how much I have learned since the beginning of my senior year—growth made possible by my determination to understand the field of computational biology.

Bibliography

- [1] Gary An, Qi Mi, Joyeeta Dutta-Moscato, and Yoram Vodovotz, *Agent-based models in translational systems biology*, WIREs Systems Biology and Medicine **1** (2009), no. 2, 159–171.
- [2] Katie Bentley, Holger Gerhardt, and Paul A. Bates, *Agent-based simulation of notch-mediated tip cell selection in angiogenic sprout initialisation*, Journal of Theoretical Biology **250** (2008), no. 1, 25–36.
- [3] Maria A. Blasco, *Telomeres and human disease: Ageing, cancer and beyond*, Nature Reviews Genetics **6** (2005), no. 8, 611–622.
- [4] Eric Bonabeau, *Agent-based modeling: Methods and techniques for simulating human systems*, Proceedings of the National Academy of Sciences **99** (2002), no. suppl3, 7280–7287.
- [5] N. E. Campbell, L. Kellenberger, J. Greenaway, R. A. Moorehead, N. M. Linnerth-Petrik, and J. Petrik, *Extracellular matrix proteins and tumor angiogenesis*, Journal of Oncology **2010** (2010), 1–13.
- [6] Arvind K. Chavali, Erwin P. Gianchandani, Kenneth S. Tung, Michael B. Lawrence, Shayn M. Peirce, and Jason A. Papin, *Characterizing emergent properties of immunological systems with multi-cellular rule-based computational modeling*, Trends in Immunology **29** (2008), no. 12, 589–599.
- [7] D. A. Cheresh and D. G. Stupack, *Regulation of angiogenesis: Apoptotic cues from the ecm*, Oncogene **27** (2008), no. 48, 6285–6298.
- [8] Nicolò Cogno, Cristian Axenie, Roman Bauer, and Vasileios Vavourakis, *Agent-based modeling in cancer biomedicine: Applications and tools for calibration and validation*, Cancer Biology & Therapy **25** (2024), no. 1, 2344600.
- [9] Anna Corti, Monika Colombo, Francesco Migliavacca, Jose Felix Rodriguez Matas, Stefano Casarin, and Claudio Chiastra, *Multiscale computational modeling of vascular adaptation: A systems biology approach using agent-based models*, Frontiers in Bioengineering and Biotechnology **9** (2021November), 744560.
- [10] Lisa M. Coussens and Zena Werb, *Matrix metalloproteinases and the development of cancer*, Chemistry & Biology **3** (1996), no. 11, 895–904.
- [11] Johannes T. Daub and Roeland M. H. Merks, *Cell-based computational modeling of vascular morphogenesis using tissue simulation toolkit*, Vascular morphogenesis, 2014, pp. 67–127.
- [12] Alicia R Folgueras, Alberto M Pendas, Luis M Sanchez, and Carlos Lopez-Otin, *Matrix metalloproteinases in cancer: from new functions to improved inhibition strategies*, International Journal of Developmental Biology **48** (2004), no. 5-6, 411–424.

- [13] Douglas Hanahan and Robert A Weinberg, *Hallmarks of cancer: the next generation*, *cell* **144** (2011), no. 5, 646–674.
- [14] Christopher D Hartman, Brett C Isenberg, Samantha G Chua, and Joyce Y Wong, *Extracellular matrix type modulates cell migration on mechanical gradients*, *Experimental cell research* **359** (2017), no. 2, 361–366.
- [15] Manoj Kumar Jena and Jagadeesh Janjanam, *Role of extracellular matrix in breast cancer development: a brief update*, *F1000Research* **7** (2018), 274.
- [16] Laxminarayanan Krishnan, James B Hoying, Hoa Nguyen, Helen Song, and Jeffrey A Weiss, *Interaction of angiogenic microvessels with the extracellular matrix*, *American Journal of Physiology-Heart and Circulatory Physiology* **293** (2007), no. 6, H3650–H3658.
- [17] Jaxson R. Libby, Haley Royce, Sarah R. Walker, and Linqing Li, *The role of extracellular matrix in angiogenesis: Beyond adhesion and structure*, *Biomaterials and Biosystems* **15** (2024September), 100097.
- [18] Sensen Lin, Shuying Wan, Li Sun, Jialiang Hu, Dongdong Fang, Renping Zhao, Shengtao Yuan, and Luyong Zhang, *Chemokine c - c motif receptor 5 and c - c motif ligand 5 promote cancer cell migration under hypoxia*, *Cancer Science* **103** (2012), no. 5, 904–912.
- [19] Tomas Lindahl and Richard D. Wood, *Quality control by dna repair*, *Science* **286** (1999), no. 5446, 1897–1905.
- [20] Roberta Lugano, Mohanraj Ramachandran, and Anna Dimberg, *Tumor angiogenesis: Causes, consequences, challenges and opportunities*, *Cellular and Molecular Life Sciences* **77** (2020), no. 9, 1745–1770.
- [21] Charles M. Macal and Michael J. North, *Agent-based modeling and simulation*, n.d. Unpublished or not associated with a journal. More publication details may be needed.
- [22] Steven R. McDougall, Alexander R. A. Anderson, and Mark A. J. Chaplain, *Mathematical modelling of dynamic adaptive tumour-induced angiogenesis: Clinical implications and therapeutic targeting strategies*, *Journal of Theoretical Biology* **241** (2006), no. 3, 564–589.
- [23] Florian Milde, Michael Bergdorf, and Petros Koumoutsakos, *A hybrid model for three-dimensional simulations of sprouting angiogenesis*, *Biophysical journal* **95** (2008), no. 7, 3146–3160.
- [24] Maurizio Mongiat, Eva Andreuzzi, Giulia Tarticchio, and Alice Paulitti, *Extracellular matrix, a hard player in angiogenesis*, *International Journal of Molecular Sciences* **17** (2016), no. 11, 1822.
- [25] Masoud Najafi, Bagher Farhood, and Keywan Mortezaee, *Extracellular matrix (ecm) stiffness and degradation as cancer drivers*, *Journal of Cellular Biochemistry* **120** (2019), no. 3, 2782–2790.
- [26] Anna Neve, Francesco Paolo Cantatore, Nicola Maruotti, Addolorata Corrado, and Domenico Ribatti, *Extracellular matrix modulates angiogenesis in physiological and pathological conditions*, *BioMed Research International* (2014), 1–10.
- [27] Kerri-Ann Norton, Kideok Jin, and Aleksander S. Popel, *Modeling triple-negative breast cancer heterogeneity: Effects of stromal macrophages, fibroblasts and tumor vasculature*, *Journal of Theoretical Biology* **452** (2018September), 56–68.
- [28] Kerri-Ann Norton and Aleksander S. Popel, *Effects of endothelial cell proliferation and migration rates in a computational model of sprouting angiogenesis*, *Scientific Reports* **6** (2016), no. 1, 36992.
- [29] Kerri-Ann Norton, Travis Wallace, Niranjan B. Pandey, and Aleksander S. Popel, *An agent-based model of triple-negative breast cancer: The interplay between chemokine receptor ccr5 expression, cancer stem cells, and hypoxia*, *BMC Systems Biology* **11** (2017), no. 1, 68.
- [30] Megan M. Olsen and Hava T. Siegelmann, *Multiscale agent-based model of tumor angiogenesis*, *Procedia Computer Science* **18** (2013), 1016–1025.
- [31] Markus R. Owen, Tomás Alarcón, Philip K. Maini, and Helen M. Byrne, *Angiogenesis and vascular remodelling in normal and cancerous tissues*, *Journal of Mathematical Biology* **58** (2009), no. 4–5, 689–721.
- [32] Ioannis Politopoulos, *Review and analysis of agent-based models in biology*, 2007. Unpublished or not associated with a journal. More publication details may be needed.
- [33] Amina A Qutub, Feilim Mac Gabhann, Emmanouil D Karagiannis, Prakash Vempati, and Aleksander S Popel, *Multiscale models of angiogenesis*, *IEEE engineering in medicine and biology magazine* **28** (2009), no. 2, 14–31.
- [34] Amina A Qutub and Aleksander S Popel, *Elongation, proliferation & migration differentiate endothelial cell phenotypes and determine capillary sprouting*, *BMC systems biology* **3** (2009), 1–24.
- [35] Mehdi Rajabi and Shaker Mousa, *The role of angiogenesis in cancer treatment*, *Biomedicines* **5** (2017), no. 2, 34.

- [36] Eun Bo Shim, Young-Guen Kwon, and Hyung Jong Ko, *Computational analysis of tumor angiogenesis patterns using a two-dimensional model*, Yonsei Medical Journal **46** (2005), no. 2, 275–283.
- [37] A. Stéphanou, A.C. Lesart, J. Deverchère, A. Juhem, A. Popov, and F. Estève, *How tumour-induced vascular changes alter angiogenesis: Insights from a computational model*, Journal of Theoretical Biology **419** (April 2017), 211–226.
- [38] Malin Sund, Liang Xie, and Raghu Kalluri, *The contribution of vascular basement membranes and extracellular matrix to the mechanics of tumor angiogenesis*, APMIS **112** (2004), no. 7–8, 450–462.
- [39] James E. Talmadge and Issiah J. Fidler, *AACR Centennial Series: The Biology of Cancer Metastasis: Historical Perspective*, Cancer Research **70** (2010), no. 14, 5649–5669.
- [40] Rui DM Travasso, Eugenia Corvera Poiré, Mario Castro, Juan Carlos Rodríguez-Manzaneque, and Aurora Hernández-Machado, *Tumor angiogenesis and vascular patterning: a mathematical model*, PloS one **6** (2011), no. 5, e19989.
- [41] Victor W. M. Van Hinsbergh, *Angiogenesis: Basics of vascular biology*, Vascularization for tissue engineering and regenerative medicine, 2016, pp. 1–29.
- [42] Karen H. Vousden and Xin Lu, *Live or let die: The cell's response to p53*, Nature Reviews Cancer **2** (2002), no. 8, 594–604.
- [43] Cameron Walker, Elijah Mojares, and Armando Del Río Hernández, *Role of extracellular matrix in development and cancer progression*, International Journal of Molecular Sciences **19** (2018), no. 10, 3028.
- [44] J. Walpole, J. C. Chappell, J. G. Cluceru, F. Mac Gabhann, V. L. Bautch, and S. M. Peirce, *Agent-based model of angiogenesis simulates capillary sprout initiation in multicellular networks*, Integrative Biology **7** (2015), no. 9, 987–997.
- [45] World Health Organization, *Cancer*, 2022. Accessed: 2025-04-30.